2008

Non-linear Shunting of Piezo-actuators for Vibration Suppression

Anisetti Anusha
Wright State University

Non-linear Shunting of Piezo-actuators for Vibration Suppression

A thesis submitted in partial fulfillment
of the requirements for the degree of
Master of Science in Engineering

by

Anusha Anisetti
Department of Mechanical and Materials Engineering
Wright State University

2007
Wright State University

Wright State University
SCHOOL OF GRADUATE STUDIES

April 21, 2008

I HEREBY RECOMMEND THAT THE THESIS PREPARED UNDER MY SUPERVISION BY Anusha Anisetti ENTITLED Non-linear Shunting of Piezo-actuators for Vibration Suppression BE ACCEPTED IN PARTIAL FULFILLMENT OF THE REQUIREMENTS FOR THE DEGREE OF Master of Science in Engineering.

Joseph C. Slater
Thesis Director

George Huang
Department Chair

Committee on
Final Examination

Joseph C. Slater, Ph.D., P.E.

Nathan Klingbeil, Ph.D.

Tommy J. George Jr, Ph.D.

Joseph F. Thomas, Jr., Ph.D.
Dean, School of Graduate Studies

ABSTRACT

Anisetti, Anusha. M.S., Department of Mechanical and Materials Engineering, Wright State University, 2007. *Non-linear Shunting of Piezo-actuators for Vibration Suppression.*

Vibrations at a resonant frequency lead to catastrophic failure or at the very least, shorten the life span of the structure due to fatigue. These problems force engineers to implement damping techniques. Smart materials have been used over two decades to reduced vibration amplitudes. Recently, there has been much research and development on smart materials and structures.

This work introduces an innovative approach for vibration suppression using passively shunted piezolectric materials. Initially linear circuit elements such as resistors, capacitors, and inductances, or building a non-linear circuit with different impedance designs were used. Instead of such elements, a switched electromechanical shunt has been proposed as a method to suppress vibrations of mechanical structures. In this state switching technique, bonded piezoelectric elements are switched from open circuit to closed circuit depending on the voltage produced from the piezoelectric patch. This new shunt circuit utilizes diodes. Diodes are nonlinear circuit elements and vibration amplitude is reduced due to introduction of nonlinearity into the system.

A physics-based electro-mechanical model is developed and validated against experimental results. The smart plate consists of a rectangular aluminum plate modeled in cantilever configuration with surface bonded piezoelectric patches. Basic equations for piezoelectric sensors and actuators are presented. The equation of motion for the plate structure with bonded piezoelectric patch is depicted. The implementation of the circuit is demonstrated analytically and experimentally. The concept is demonstrated on two different modes and vibration peaks are lowered using the above mentioned circuit.

Then a numerical model of the plate with the piezoelectric patch and the circuit is built in Simulink after designing a finite element model in ABAQUS. The data shows the effect of damping in Frequency Response Functions (FRFs) and in the response plots. A state-space model is also developed. Simulations of the model are compared to the experimental results.

The results indicate the feasibility of the smart damping materials for many industrial applications where reducing noise and vibrations are desired. It is clear that the maximum suppression that

can be obtained with this method is dependent on the voltage drop across the piezoelectric element.

List of Symbols

A_p	Area of the piezoelectric patch (m^2)
t_p	Thickness of the piezoelectric patch (m)
S_p	Strain (m/m)
s_{pq}	Elastic compliance (m^2/N)
T_q	Stress (N/m^2)
d_{kp}	Piezoelectric strain constant (m/V)
E_k	Electric field (V/m)
D_i	Charge-density (Coulomb/m^2)
Q	Charge (coloumb)
ϵ_{ik}	Permittivity (F/m)
$i(t)$	Current (amp)
$v(t)$	Voltage (Volts)
V_{th}	Thermal voltage (Volts)
k	Boltzmann constant (J/K)
T	Temperature (K)
q	Charge on electron (Coulomb)
I_o	Leakage current (amp)

Contents

List of Figures

List of Tables

Acknowledgement

I would like to thank my advisor Joseph C. Slater, for giving this opportunity to work with him. He has supported and accompanied me throughout my thesis work. His integral view on research has inspired me. I owe him lots of gratitude for having shown me this way of research.

I would also like to gratefully acknowledge the support of some very special individuals, Steven Page and Oleg Shiryayev. They helped me immensely in my experimental work and mirrored back my ideas so I heard them aloud. I am very much thankful to them.

To my parents, who supported me to come here and study in an esteemed University. Their belief and love allowed me the freedom to pursue my Masters.

Dedicated to

My Parents

Introduction

1.1 Motivation

Mechanical systems are often of high order and may contain a large number of lightly damped modes. The modeling and control design for such systems is well known to pose significant challenges. It is prudent to introduce damping into a system to achieve a satisfactory response from the structure. New concepts of enhancing the structural damping characteristics were introduced by smart materials. They have drawn close attention from the structural dynamics community in the past few decades ((1), (2)). Augmenting the benefits of the piezoelectric materials for structural damping, immense interest is placed on acoustic control, structural health monitoring and many other applications. Design aspects, depend on the actual actuation required and the type of suppression needed.

Systems whose actuation mechanisms display both direct, i.e., mechanical work to electrical energy conversion, and converse effects between electrical charge and mechanical work, employ electromechanical effects. Piezoelectric materials are one such type of material, they are anisotropic. When piezoelectric material is subjected to mechanical stress, it results in deformation thus producing electric charge. This is called the "Piezoelectric Effect." Originally, these patches were used to amplify the voltage signals produced from the strain as in audio amplifiers. Now they are used in a wide variety of applications ranging from control of aerospace structures to the development of increased performance of mechanical devices.

With the advancement of smart material technology, smaller actuators and sensors have been created and incorporated into structures for structural damping. Materials to be used for sensing and

actuation are usually manufactured in several common geometries including discs, rings, cylinders, and square plates. They can be either glued on or embedded ((1)) into the structure that is to be controlled. The particular technique used in this thesis work is a position based sensing technique using a rectangular patch glued onto a plate.

1.2 Background Research

Research Objectives

The main objectives of this study are:

- Determine a new passive electrical shunt for structural damping.
- Find how piezoelectric patches may be used to counteract fundamental resonant peaks.
- Compare experimental results with predictions.

Many different damping mechanisms were proposed during these years of research on smart material damping. (1) Active Damping, (2) Passive Damping and (3) Active-Shunted Hybrid Damping

1.2.1 Active Damping

Two piezoelectric patches, sensor and actuator, are attached to the host-structure for smart damping. Active damping in simple words is obtained by using an actuator and sensor acting in a closed loop ((3), (4)). Active devices or controllers generally comprise a distinct set of sensor circuitry, drive circuitry and actuator circuitry. Voltage obtained on the sensor is transferred to the actuator thus opposing the vibration of the structure and achieving active damping. When the host-structure vibrates, its motion is sensed by the piezoelectric sensor attached. This sensed vibration signal is then amplified and fed back through feed-back controllers as shown in Figure 1.1. ((5))

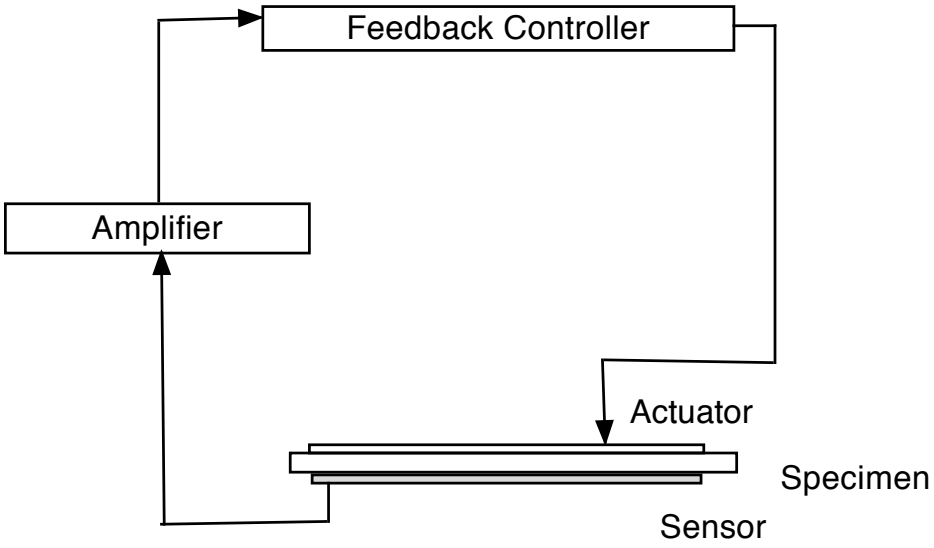

Figure 1.1: Active vibration control

Although active suppression techniques using piezoelectric actuators may allow larger amplitude reduction, they are more cumbersome to implement. A major concern in active damping is the stability problems that may arise due to control spill-over as explained by Meirovitch (6) due to failure of sensors and actuators. This technique can be very sensitive to uncertainties and variations of system parameters ((7)). Active damping requires complex amplifiers, complicated algorithms and associated sensing electronics which poses a limitation to its practical use in applications where low cost is a critical necessity.

1.2.2 Passive Damping

Passive damping ((8)) works on the concept of energy dissipation as shown in 1.2. The principle of passive damping is as simple as the following: when a mechanical disturbance is induced in the structure, it strains the piezoelectric patch attached to it, thus generating electrical energy. Electrical energy is then dissipated, or otherwise altered, through a shunting circuit before it reverts to the mechanical system.

Shunting circuits may contain many electrical components in different combinations. Resistors, capacitors and inductors have already been used as passive control electrical components. Hagood and Von Flotow ((9)), investigated the piezoelectric shunt using a resistor and inductor in

series. More piezoelectric dampers shunted with a resistor and inductor in parallel were studied by Wu, ((10)). These electrical absorbers can be used to suppress either a single mode or multiple modes ((11)) at once. The advantage of this approach is that the shunt circuit can be easily placed on the structure together with the piezoelectric patch.

Generally, for broadband damping, a resistor is shunted across a direct effect mechanism, which is typically a piezo-capacitor. For narrow band damping, both an inductor and a resistor must be shunted across the device to form a resonant LRC circuit. This circuit is usually tuned to a resonant frequency of the structure to be damped. In a resistively shunted circuit, the resistance is varied until the circuit time constant is close to the modes to be damped. The primary difficulty with resistive shunted circuits is the dissipation of sufficient energy and need for large resistance values to dissipate large amounts of energy. A non-linear circuit with different impedance designs ((12)), has been proposed as one the passive damping techniques.

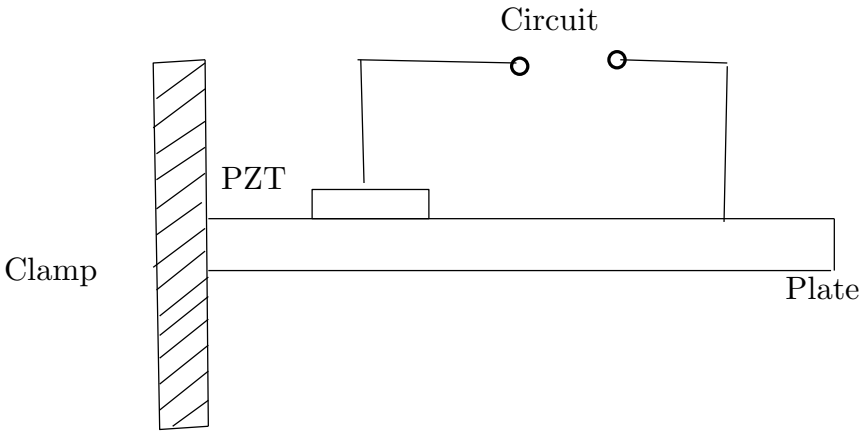

Figure 1.2: Passive vibration control

The advantage of passive damping is that the shunt circuit can be easily embedded in the structure together with the piezoelectric patch. This technique does not require complex amplifiers and can be easily tuned ((13)) for the frequency to be suppressed comparative to the active damping technique.

1.2.3 Active-Shunted Hybrid Damping

The configuration of hybrid piezoelectric absorber ((14)) generally integrates piezoelectric elements with an active control voltage source and a shunt circuit. Active inductors are synthesized using op-amps and other components to implement piezoelectric vibration absorbers in this case. This sort of damping is also known as semi-active. Tsai and Wang ((15)) discussed the issues of the active-shunted hybrid type of piezoelectric damping system. They also illustrated that the shunting circuit can enhance the active actuation for structural vibration suppression and therefore active-shunted hybrid damping is more effective than separated active and passive damping mechanisms. Garg and Anderson ((16)) advanced the hybrid active-passive technology. Switching control of hybrid piezoelectric damper was also demonstrated by Adachi, Awakura, and Iwatsubo ((17)). They proved that variable hybrid piezoelectric damping is more effective than the regular hybrid piezoelectric damping.

The major advantage of active shunted hybrid damping is the reduction in control effort by active control and simplicity of the implementation loop, which uses only analog elements for real-time testing. Both the advantages of active and passive damping techniques are incorporated thus improving the overall stability of the system. But aforementioned problems with respect to purely active control, namely, lack of efficiency, energy consumption, and heat dissipation reoccur.

1.3 Thesis Overview

Smart materials possess an exploitable coupling between mechanical or elastic quantities such as stress and strain, and other extra-mechanical quantities involving electric, magnetic, thermal and other fields. By correctly employing these properties, it is possible to incorporate smart materials into structures, to introduce unique functionality.

To suppress vibration using this functionality is the main goal of this Thesis. This work introduces new passive elements to achieve vibration damping.

The previous section discussed various ways used to suppress the vibration using piezoelectric patches. Different means of damping techniques using smart materials are also described.

In Chapter 2, the experimental hardware required for the task is discussed. The description of the specimen (an aluminum plate) and the contrivances used to achieve this goal is also presented. Section 2.1 elucidates the finite element modeling of the specimen. Section 2.2 explains the experimental setup used and the data acquisition system used to obtain the experimental results.

The thesis progresses in the following way. In Chapter 3, the vital role of the bond between the piezoelectric patch and host structure are explained in Section 3.1. Piezoelectricity and its properties, assumptions (3.2) made to use them are remarked. Section 3.4 discusses the relationship between the mechanical model and the constitutive equations of the piezoelectric patch. Finite element formulation, and an analytical model of the use of the piezoelectric patch in our case are illustrated. The computation of analytical natural frequencies from the finite element model of the plate is explained in Section 3.5. The System Equivalent Reduction Process SEREP that is used to obtain a reduced model of the plate is explained in this chapter. Static Condensation is utilized to reduce the model corresponding to the electrical degrees of freedom. Guyan reduction is used only for the volt degrees of freedom as it has no inertia terms. This reduction process is not used to reduce the system reduction for the rotations and translational degrees of freedom because the significance of inertia terms increases with the increasing driving frequency. The frequency response functions generated using Guyan reduction are good only at zero driving frequency.

Preliminary design for the test specimen is presented. Chapter 4, verifies if the experimental set up meets the required conditions to run the tests. The effects of the surroundings and boundary conditions are interpreted. The clamp and the shaker used are tested for possible responses that may interact with later experiments in Sections 4.1 and 4.2.

In Chapter 5, passive circuit elements are discussed. The way they impose damping into the host structure by dissipating the energy from the piezoelectric patch is demonstrated. A self-sensing technique using non-linear circuit elements (Section 5.1.1) to acquire passive damping is designed. This design is used to attenuate the first mode and the two-stripe mode (6^{th} mode) of vibration of the cantilevered plate.

Chapter 6 goes through the application system identification technique to entire system. The work provided in this chapter is analytical. Simulink, a software available with MATLAB is used

to model the system and optimize for the electrical elements used.

All the results attained are illustrated in Chapter 7. Section 7.1 demonstrates the experimental results obtained by running sine sweeps. The purpose of the Simulink model development and test results performed recently are explained.

Finally, in Chapter 8, in the conclusion, the accomplishments of the work described in this thesis work, and suggest some possible future directions. It also mentions some of the visual observations from the experiments.

Experiment Setup

To achieve the objectives of this study, a rectangular aluminum plate is clamped to a shaker and vibrated accordingly. The output from the amplifier is connected to the shaker. The power amplifier of the shaker provides the necessary power levels through the operating frequency range so that the shaker produces a controlled level of Force.

2.1 Specimen

The specimens are rectangular plates of dimensions 9 in. $\times$ 3.5 in., made of AL6061-T6. They are 1 mm in thickness. The plate is clamped at one end so that the protruded plate is of size 8 in. $\times$ 3.5 in.

2.2 Setup

A holding device shown in Figure 2.1 was designed to allow the specimen to be clamped at one end. This clamped end would then go onto the shaker head. This clamp is a two piece device with one part bolted onto the shaker head and both the parts bolted together to hold the specimen between them. The bolts joining the two parts of the clamp are tightened enough so that it can be assumed to have clamped boundary conditions at one end of the specimen. **M6**$\times$**25** mm counter sunk bolts are used to hold the clamp onto the shaker. The upper piece of the clamp is then bolted to the lower piece using two **M8**$\times$**45** mm bolts. These bolts are placed at a distance of 14cm apart so that they do not touch the base of the shaker head and have enough space to place the plate of width 3.5in.

The fixture is tightened enough to clasp the specimen (rectangular plate 9"×3.5"), so that it is a cantilever plate of dimensions 8"×3.5."

ITEM NO.	PART NUMBER	DESCRIPTION	QTY.
1	TOP PLATE		1
2	BOTTOM PLATE		1

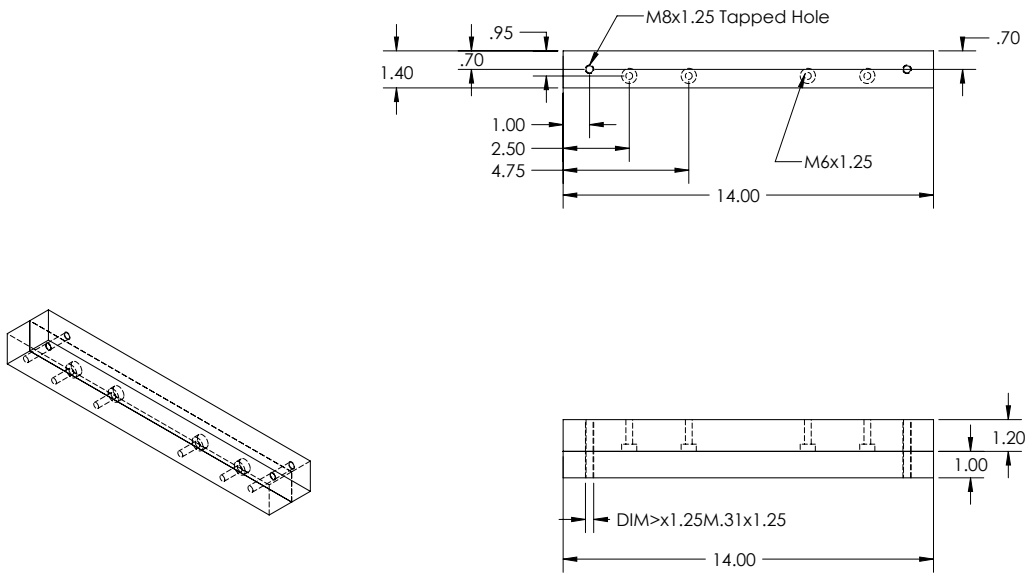

Figure 2.1: Clamp to fix the specimen on shaker

2.2.1 Shaker

A vibration generating system (Unholtz-Dickie S032 Shaker) is used to vibrate the specimen. It consists of three separate parts: the shaker, the power amplifier and the control console.

The shaker used in our experiment is pedestal based and vibrates perpendicular to its surface. The intensity of the force generated by the shaker head depends upon the items attached to the table and the operating conditions. The table movement is determined by the magnitude and frequency of the drive signal from the vibration controller. Vibration is controlled using a digital signal processing unit. The output from the signal processing unit is connected to the power amplifier governing the output acceleration from the shaker i.e., generate a controlled level of force.

The power amplifier input is connected to the controlling drive signal source and the output is connected to the drive coils of the shaker. The controller generates a low power, low voltage signal which is amplified by the electric power amplifier. The power amplifier is designed to provide the necessary power levels through operating frequency range without introduction of significant distortion. The power amplifier also contains an amplifier gain control and is used to amplify the magnitude of the signal and also to make sure that high power does not pass through the shaker as soon as it is operated.

2.2.2 Accelerometer

An ICP accelerometer, mounted on the free end of the specimen as shown in Figure 2.2, is used to attain the Frequency Response Functions of the specimen. This accelerometer also has the ability to attain the response plot. These sensors are easy to operate and interface with signal analysis and data acquisition. The best feature of ICP accelerometer is its fixed voltage sensitivity irrespective of the type or length of the cable. It can be easily glued on to the specimen using wax.

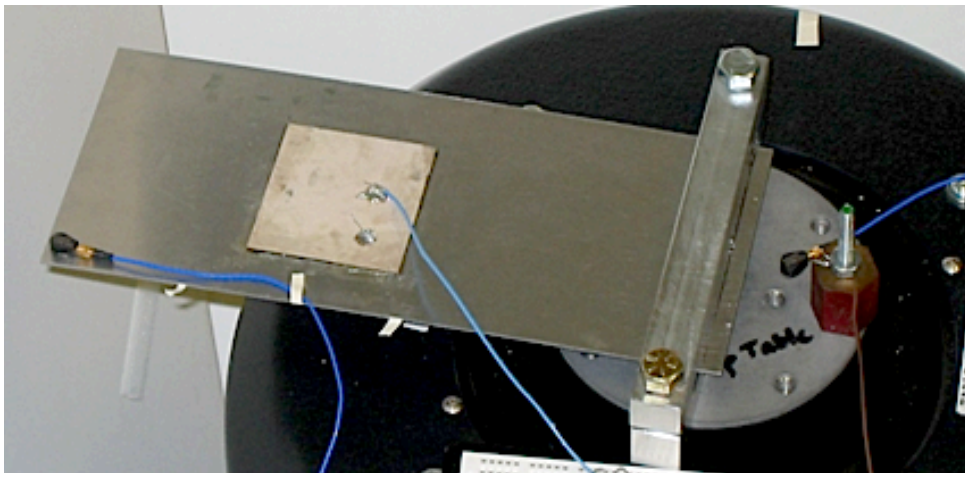

Figure 2.2: Accelerometer placed on free end of the plate

2.2.3 Data Acquisition Unit

The data acquisition digital signal processing unit used in the experiment is a Spectral Dynamics SIGLAB, model 20a. The Siglab is configured with 2 input and 2 output channels. The accelerometer placed on the plate is connected to a signal conditioner and then to the DSP unit with BNC connectors. Signal conditioning is important as it converts the voltage signal from the accelerometer to a signal that can be read by SIGLAB. The signal conditioner amplifies, isolates and linearizes the signal.

Virtual Sine Sweep (VSS) of excitation is output to the power amplifier or shaker and the accelerometer is connected to the input to attain Frequency Response Functions (FRFs). A Virtual Network Analyzer (VNA) to measure time histories, power spectrum, transfer function/FRF, coherence, etc. can also be accessed using Siglab. Siglab also has the opportunity of generating different types of functions using Virtual Function Generator (VFG).

Piezoelectric Patch

Piezoelectric sensors and actuators have drawn attention among several control research fields such as vibration suppression, shape and acoustic controls. The special property of the piezoelectric materials is they convert mechanical energy into electrical energy and vice versa. One of the main advantages of the piezoelectric patch is that they can exert control forces to host structures without any external supports. They are also light and economical and can be easily embedded into or bonded onto the host structure. Piezoelectric materials are brittle,though, susceptible to cracking, particularly when subjected to cyclic loading. They serve the purpose of vibration suppression here. De-bonding of the piezoelectric patch from the host structure can be an important problem for reliable and safe operation of smart structures and effects on the overall performance of the smart structure. Problems arising due to de-bonding are discussed by Tong, Sun and Atluri, ((18)).

In most cases, multiple piezoelectric sensors and actuators are used and distributed over specific locations of the controlled structure. Applying a designed control method, these actuators apply control forces to the structure to deform into required shape or maintain in a level of vibration. Thus placement of sensor or actuator is a major issue and the performance of the control system can be improved by optimally placing and minimizing the energy consumption. Tzou and Fu, ((19)) demonstrated that some vibrational modes can not be controlled using distributed piezoelectric sensors and actuators because of the lack of controllability. So, they divided the sensors and actuators into four patches to suppress most vibrational modes. This enhances the control efficiency and control several modes simultaneously.

3.1 Bonding of PZT

Initially, two piezoelectric patches were bonded on to the host structure, one on top and the other on the bottom to suppress a single mode. One of the patches acts like a sensor whilst other is an actuator. Various optimization methods ((20), (21)) have been developed to properly place the sensor and actuator on top and bottom of the structure to avoid problems such as lack of observability, controllability and spillover. A technique has been developed by Dosch et al. ((22)) which allows a single piece of piezoelectric material to concurrently sense and actuate in a closed-loop system. This technique is used in this experiment to measure the voltage output of the sensor. Problems arising from the capacitive coupling between the sensor and the actuator elements thus no longer exist as the self-sensing actuator is truly collocated.

For optimal placement ((23)) of the piezoelectric patch, a simple 'Sand Test' was performed on the Aluminum cantilever plate to see the nodal lines on the plate of two specific modes in this case, first mode and the first two-stripe mode. A strategic location is selected such that the piezoelectric patch is placed where maximum strain occurs.

Piezoelectric patches from Ferroperm, type Pz29, were mounted to excite the structure. Different sizes of piezoelectric patches are used to suppress different modes. A square piezoelectric patch is used to suppress the first mode whilst a rectangular piezoelectric patch is used to suppress the two- stripe mode in this experiment. The patches used have a thickness of 1mm. A five minute epoxy is used to glue the actuator to the specimen and care was taken that de-bonding does not occur. Non-conductive epoxy is used to make sure that the plate and piezoelectric patch are not short circuited around the edges of the piezoelectric patch. The patches experienced greater voltage potential in a direction normal to its surface. An electrical lead is then soldered onto the piezoelectric patch for external circuitry or passive damping while the other lead is same as the ground of the shaker. When soldering the electrical leads, it is important that the temperature does not exceed the Curie point temperature of the material because this will immediately de-pole the piezoelectric phase.

3.2 Assumptions

Mathematical models of the piezoceramic sensors or actuators are derived based on the following assumptions-

- The poling direction of the piezoelectric is in the direction normal to the surface.
- Uniform fields and displacements occur through out the piezoelectric patch.
- PZT is linearly elastic and transversely isotropic.
- The piezoelectric sensors or actuators are thin compared with plate thickness.
- Perfect bonding between piezoelectric patch and plate is considered.
- Transverse normal stress σ_z is negligible.
- Nodal accelerations are perfectly extracted from the measurements.

3.3 Constitutive Piezoelectric Equations

Piezoelectricity is a combined effect of the electrical behavior of the material and can be described mathematically within a materials constitutive equation, which defines how the piezoelectric materials stress, strain, electric displacement and electric field are related to each other and are represented as

$$S_p = s_{pq}^E T_q + d_{kp} E_k \tag{3.1}$$

$$D_i = d_{iq} T_q + \epsilon_{ik}^T E_k \tag{3.2}$$

according to (22). S_p is the strain in the piezoelectric material, T_q is the stress vector, s_{pq}^E are compliance coefficients, d_{kp} is the piezoelectric constants (or dielectric constants), E_k is the electric field, D_i is the electric charge-density displacement and ϵ_{ik}^T are electric permittivity in 3-D. The superscripts E and T denote the values of constants at constant electric field and stress respectively.

According to ((24)) piezoelectric matrices are described below The compliance matrix for PZT takes the for

$$s^E = \begin{bmatrix} s_{11} & s_{12} & s_{12} & 0 & 0 & 0 \\ s_{12} & s_{11} & s_{12} & 0 & 0 & 0 \\ s_{12} & s_{12} & s_{33} & 0 & 0 & 0 \\ 0 & 0 & 0 & s_{44} & 0 & 0 \\ 0 & 0 & 0 & 0 & s_{44} & 0 \\ 0 & 0 & 0 & 0 & 0 & 2(s_{11} - s_{12}) \end{bmatrix} \tag{3.3}$$

Piezoelectric constants and relative permittivity matrices are in the form,

$$\mathbf{d} = \begin{bmatrix} 0 & 0 & 0 & 0 & d_{15} & 0 \\ 0 & 0 & 0 & d_{15} & 0 & 0 \\ d_{31} & d_{31} & d_{33} & 0 & 0 & 0 \end{bmatrix} \quad \epsilon = \begin{bmatrix} \epsilon_{11} & 0 & 0 \\ 0 & \epsilon_{11} & 0 \\ 0 & 0 & \epsilon_{33} \end{bmatrix} \tag{3.4}$$

Equation (3.2) states that the electric displacement is proportional to both the applied stress and the applied electric field. Equation (3.1) gives the strain in the piezoelectric patch due to mechanical stress and the applied electric field. Finally s, d, ϵ are constant terms, that couple both mechanical and electrical equations by virtue of dielectric effect and piezoelectric effect. The first term in the subscripts of the piezoelectric constants refers to the electrical axis while the second refers to the mechanical axis. Equations (3.2) and (3.1) represent relations for the 3-dimensional case.

3.4 Mathematical Formulation

Now, using the traditional concepts of electrical admittance, it is easy to perform a change of variables that can be used in the electro-mechanical equations given above. If t_p and A_p are the thickness and area of the piezoelectric patch respectively, then with the help of definitions of voltage, current and charge density by (25):

$$V_i = \int_0^{t_p} E dt_p \tag{3.5}$$

$$Q = \int I dt \tag{3.6}$$

$$D = \frac{Q}{A_p} \tag{3.7}$$

Substituting solved equation (3.5) and equations (3.7) into (3.1) and (3.2) we obtain

$$S_p = s^E_{pq} T_q + \frac{d_{kp} V_k}{t_p} \tag{3.8}$$

$$Q_i = d_{iq} A_p T_q + \frac{\epsilon_{ik} A_p}{t_p} V_k \tag{3.9}$$

3.5 Finite Element Model

A finite element formulation for plate elements is performed in ANSYS. The plate element used has 4 nodes along the edges with no nodes in the interior (i.e., serendipity elements). All functions derived are based on the iso-parametric element as shown in Figure 3.1 in intrinsic coordinates. It is a square plate element with sides 2 and 2 in ξ and η directions respectively. Nodes are numbered as in the Figure 3.1. It has three degrees of freedom at each node, one translation in ζ direction, $w_i(\xi,\eta)$, and two rotations $\frac{\partial w}{\partial \xi}$, $\frac{\partial w}{\partial \eta}$. The element nodal displacement vector of the plate is thus of the order of 12 $\times$1 and is given as

$$\delta = \begin{pmatrix} w_1 & \theta_{\text{x1}} & \theta_{\text{y1}} & w_2 & \theta_{\text{x2}} & \theta_{\text{y2}} & w_3 & \theta_{\text{x3}} & \theta_{\text{y3}} & w_4 & \theta_{\text{x4}} & \theta_{\text{y4}} \end{pmatrix}^T \tag{3.10}$$

Plate element lateral displacement w is interpolated with the shape functions N_i and nodal displacements δ_i.

$$w = \mathbf{N}\delta \tag{3.11}$$

or in terms of a polynomial

$$w = PA \tag{3.12}$$

where

$$P = \begin{pmatrix} 1 & \xi & \eta & \xi^2 & \xi\eta & \eta^2 & \xi^3 & \xi^2\eta & \xi\eta^2 & \eta^3 & \xi^3\eta & \xi\eta^3 \end{pmatrix} \tag{3.13}$$

and A is a vector of constant terms

$$A = \begin{pmatrix} A_1 & A_2 & A_3 & A_4 & A_5 & A_6 & A_7 & A_8 & A_9 & A_{10} & A_{11} & A_{12} \end{pmatrix}^T \tag{3.14}$$

Substituting the nodal coordinates in Equation 3.12, a set of 12 equations in terms of 12 constant

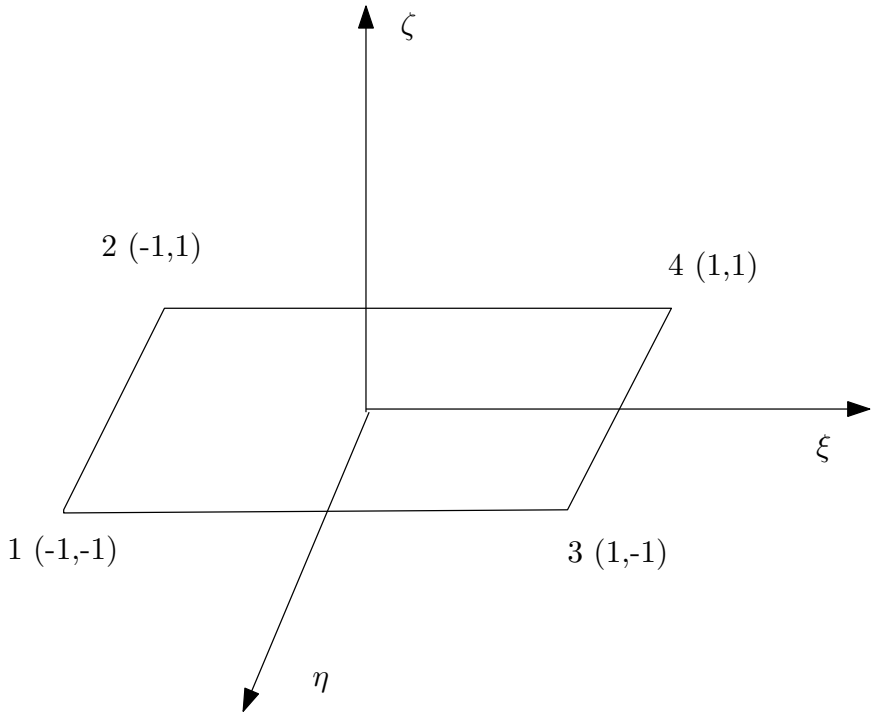

Figure 3.1: Plate element in intrinsic coordinates

terms is acquired. These equations are further solved for the constant terms and are substituted back into the Equation 3.12, thus generating the shape functions for the four node plate element (Figure

3.1) as given below

$$\mathbf{N} = \frac{1}{8}\begin{bmatrix} (2-3*\xi-3*\eta+4*\xi*\eta+\xi^3+\eta^3-\xi^3*\eta-\xi*\eta^3) \\ (1-\xi-\eta+\xi*\eta-\eta^2+\xi*\eta^2+\eta^3-\xi*\eta^3) \\ (-1+\xi+\eta+\xi^2-\xi*\eta-\xi^3-\xi^2*\eta+\xi^3*\eta) \\ (2+3*\xi-3*\eta-4*\xi*\eta-\xi^3+\eta^3+\xi^3*\eta+\xi*\eta^3) \\ (1-\xi-\eta-\xi*\eta-\eta^2-\xi*\eta^2+\eta^3+\xi*\eta^3) \\ (1+\xi-\eta-\xi^2-\xi*\eta-\xi^3+\xi^2*\eta+\xi^3*\eta) \\ (2+3*\xi+3*\eta+4*\xi*\eta-\xi^3-\eta^3-\xi^3*\eta-\xi*\eta^3) \\ (-1-\xi-\eta-\xi*\eta+\eta^2+\xi*\eta^2+\eta^3+\xi*\eta^3) \\ (1+\xi+\eta-\xi^2+\xi*\eta-\xi^3-\xi^2*\eta-\xi^3*\eta) \\ (2-3*\xi+3*y-4*\xi*\eta+\xi^3-\eta^3+\xi^3*\eta+\xi*\eta^3) \\ (-1+\xi-\eta+\xi*\eta+\eta^2-\xi*\eta^2+\eta^3-\xi*\eta^3) \\ (-1+\xi-\eta+\xi^2+\xi*\eta-\xi^3+\xi^2*\eta-\xi^3*\eta) \end{bmatrix} \tag{3.15}$$

With the help of the above shape functions, stiffness and mass matrices of the plate can be determined. The element elastic stiffness matrix is evaluated from

$$[K_e] = \iint [B]^T[D][B]d\xi d\eta \tag{3.16}$$

in which [B] is the element strain matrix calculated from the shape functions as

$$B = \begin{bmatrix} -\frac{\partial^2 N}{\partial x^2} \\ \\ -\frac{\partial^2 N}{\partial y^2} \\ \\ -2\frac{\partial^2 N}{\partial x \partial y} \end{bmatrix} \tag{3.17}$$

where **N** is the array of shape functions at nodes i,j, k and l respectively. The matrix **B** in Equation 3.17 is in general coordinates and can be computed in intrinsic coordinates by determining Jacobians

as

$$\begin{bmatrix} \frac{\partial^2 N}{\partial \xi^2} \\ \\ \frac{\partial^2 N}{\partial \eta^2} \\ \\ 2\frac{\partial^2 N}{\partial \xi \partial \eta} \end{bmatrix} = \begin{bmatrix} \frac{\partial^2 x}{\partial \xi^2} & \frac{\partial^2 y}{\partial \xi^2} \\ \\ \frac{\partial^2 x}{\partial \eta^2} & \frac{\partial^2 y}{\partial \eta^2} \\ \\ \frac{\partial^2 x}{\partial \xi \partial \eta} & \frac{\partial^2 y}{\partial \xi \partial \eta} \end{bmatrix} \begin{bmatrix} \frac{\partial N}{\partial x} \\ \\ \frac{\partial N}{\partial y} \end{bmatrix} + \begin{bmatrix} \frac{\partial x}{\partial \xi}^2 & \frac{\partial x}{\partial \xi}^2 & \frac{\partial x}{\partial \xi}\frac{\partial y}{\partial \xi} \\ \\ \frac{\partial x}{\partial \eta}^2 & \frac{\partial x}{\partial \eta}^2 & \frac{\partial x}{\partial \eta}\frac{\partial y}{\partial \eta} \\ \\ \frac{\partial x}{\partial \xi}\frac{\partial x}{\partial \eta} & \frac{\partial y}{\partial \xi}\frac{\partial y}{\partial \eta} & (\frac{\partial x}{\partial \xi}\frac{\partial y}{\partial \eta} + \frac{\partial x}{\partial \eta}\frac{\partial y}{\partial \xi}) \end{bmatrix} \begin{bmatrix} \frac{\partial^2 N}{\partial x^2} \\ \\ \frac{\partial^2 N}{\partial y^2} \\ \\ 2\frac{\partial^2 N}{\partial x \partial y} \end{bmatrix} \tag{3.18}$$

where [D] is the elastic matrix of the plate element given as

$$[D] = \frac{E * t^3}{12(1-\nu^2)} \begin{bmatrix} 1 & \nu & 0 \\ \nu & 1 & 0 \\ 0 & 0 & (1-\nu)/2 \end{bmatrix} \tag{3.19}$$

where E is the Young's modulus of the plate, t is the thickness of the plate and ν is the Poisson's Ratio. The mechanical properties for the Aluminum plates (specimen) used are given in the following Table 3.1.

Table 3.1: Material Properties of Aluminum

Density(ρ)	Poisson Ratio(ν)	Young's Modulus(E)
2700 $\frac{kg}{m^3}$	0.3	73 GPa

The Mass matrix is evaluated from the general form

$$M = \rho \iint N^T N d\xi d\eta \tag{3.20}$$

The first 10 modes of the plate were first estimated by ANSYS (See Figures (3.2a, 3.2b.....3.2j). Clamped-Free boundary conditions were assumed for this modeling. This model of ANSYS helped to determine the natural frequencies of the beam which are compared to the experimental results. The experimental natural frequencies were obtained from the frequency response function obtained in the range of 0 Hz to 1000 Hz as shown in the Figure 3.3. Comparison is given in Table 3.2.

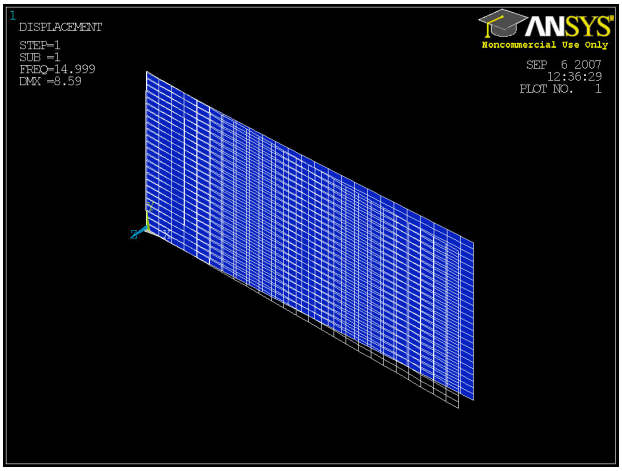

(a) First Mode

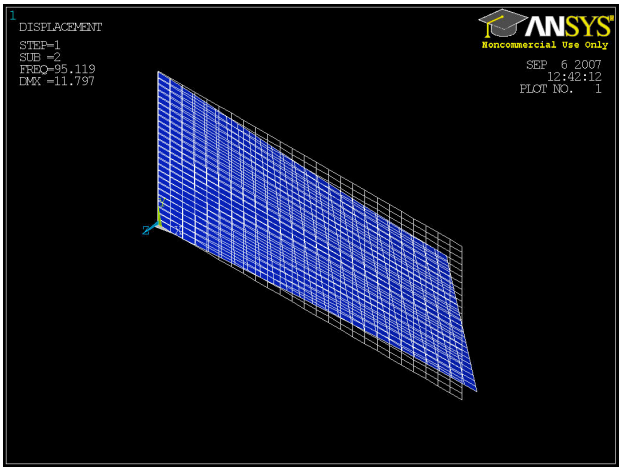

(b) Second Mode

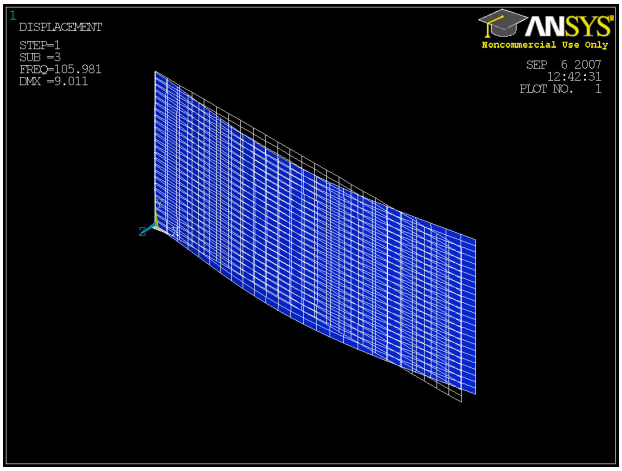

(c) Third Mode

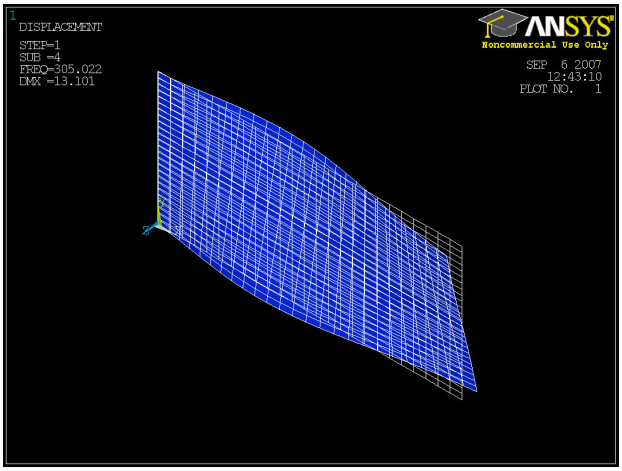

(d) Fourth Mode

Figure 3.2: Mode shapes of cantilever plate from ANSYS

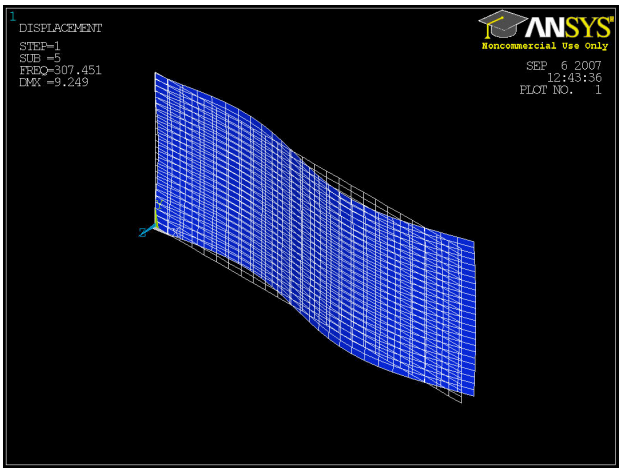

(e) Fifth Mode

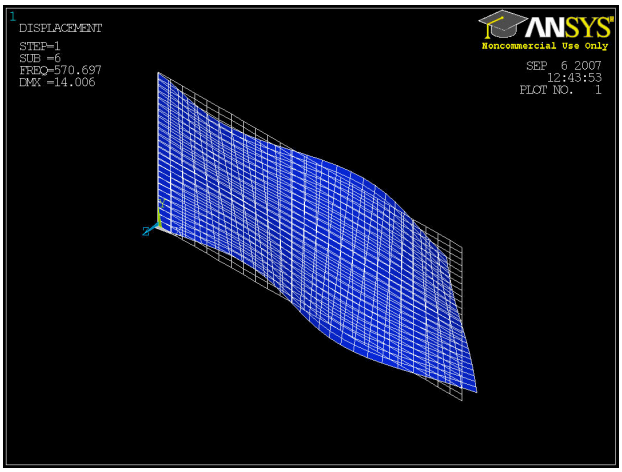

(f) Sixth Mode

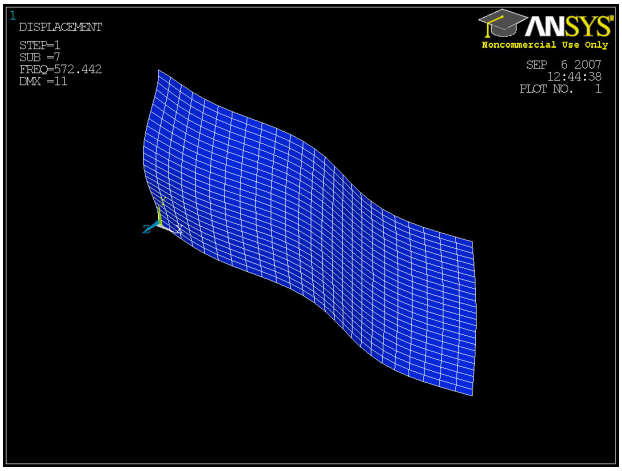

(g) Seventh Mode

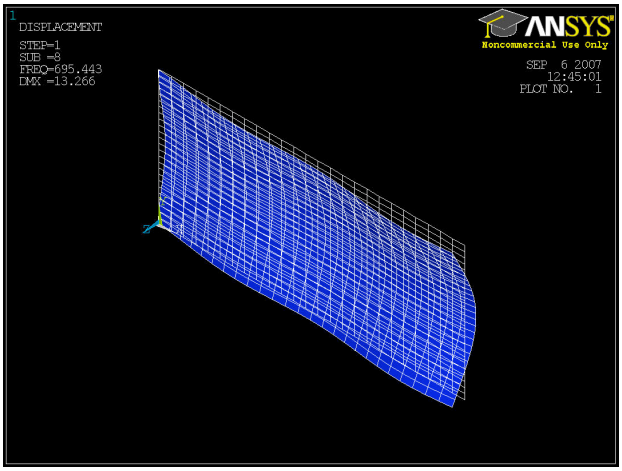

(h) Eighth Mode

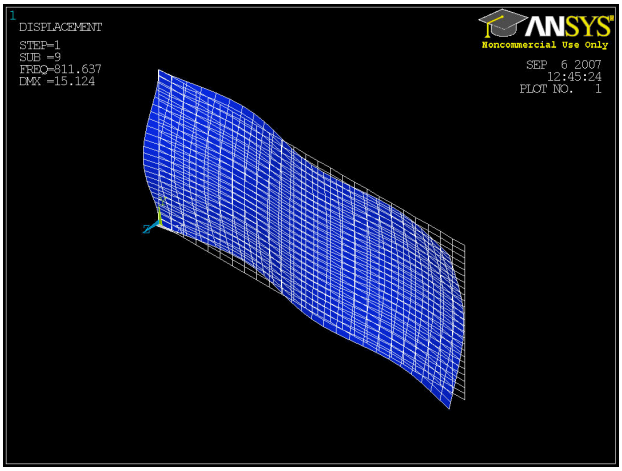

(i) Ninth Mode

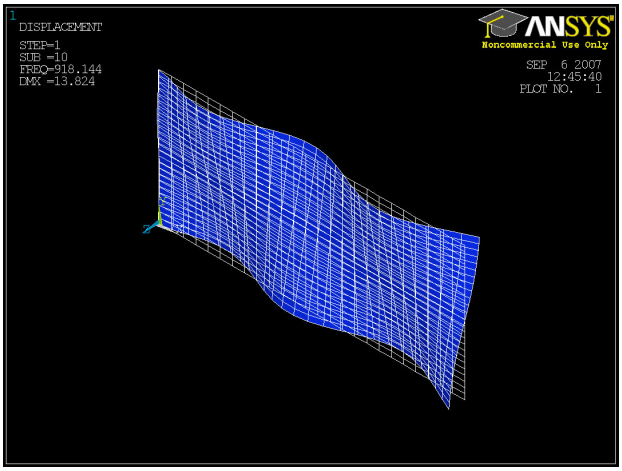

(j) Tenth Mode

Figure 3.2: Mode shapes of cantilever plate from ANSYS

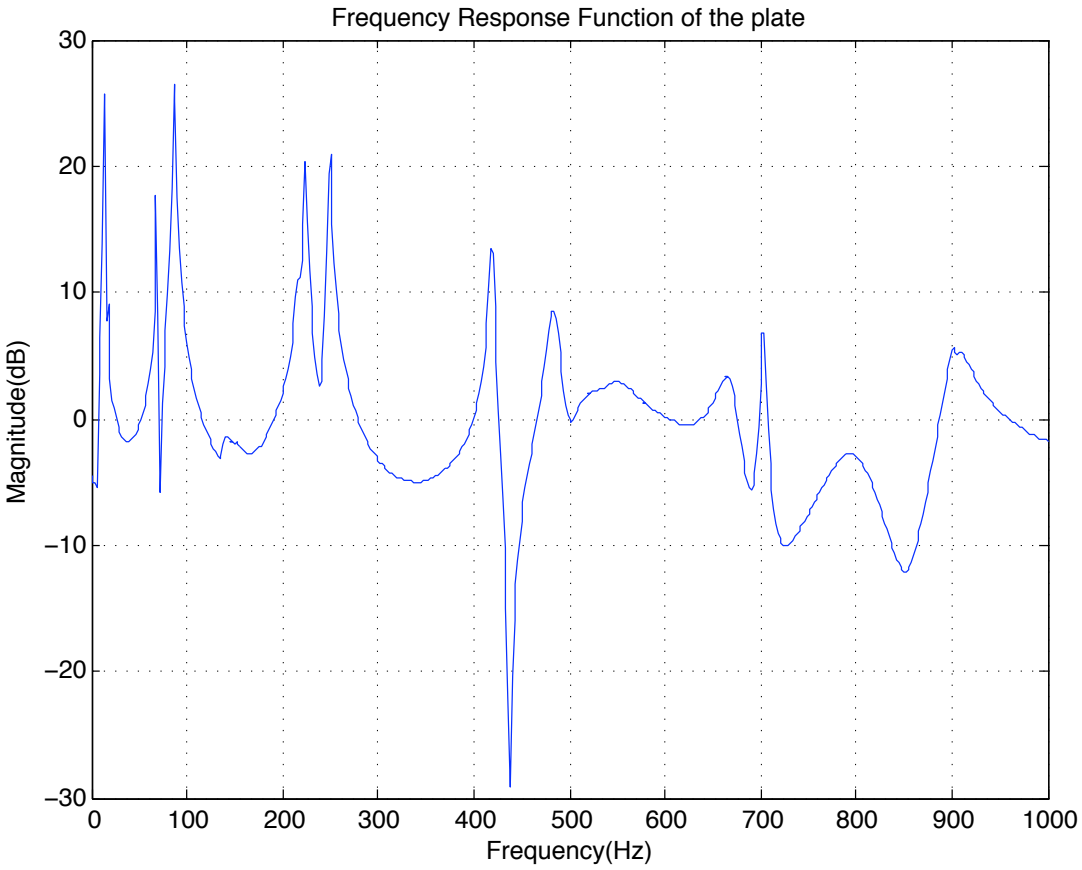

Figure 3.3: Frequency response function

Table 3.2: Natural frequencies of the cantilever plate

Set	Natural frequencies from ANSYS	Natural frequencies from EXPERIMENT
1	14.999 Hz	14.0
2	95.119 Hz	68.97
3	105.98 Hz	87.0
4	305.20 Hz	224
5	307.45 Hz	250
6	570.70 Hz	418
7	572.44 Hz	484
8	695.44 Hz	702
9	811.64 Hz	794
10	918.14 Hz	902

This model from ANSYS is useful to capture the dynamics of the plate, and determine the nodal locations for the predominant modes. The ANSYS example was used to ascertain the maximum strain area on the plate. Before placing the piezoelectric patch, the nodal lines of the test article were ascertained with a simple"Sand Test." The plate is excited at the frequency of interest and sand is slowly spread on the plate. After a while the sand over the plate forms a nice pattern of nodal lines on the plate, thus showing the optimal position to glue the piezoelectric patch on the plate to obtain effective transfer of energy and determine the influences of the actuator placement on the response.

After examining the mode shapes, piezoelectric patches were glued to the structure at the chosen. A square piezoelectric patch was attached at the center of the plate to suppress the first mode frequency as shown in Figure 3.4, while a rectangular piezoelectric patch is attached at a distance of 1in from the free end, as there is maximum strain at this place during two-stripe mode vibration. The FRF of the plate with the piezoelectric patch has higher natural frequencies as shown in Figure 3.5 because of the increased stiffness of the plate.

Modal analysis was then performed on the plate with the piezoelectric patch adhered onto the cantilevered plate using the Finite Element Package, ABAQUS. The effect of the piezoelectric patch on the natural frequencies after the piezoelectric patch is attached, to suppress the first mode, is shown in Table 3.3 and the mode shapes are depicted as in Figures (3.6a, 3.6b.....3.6j).

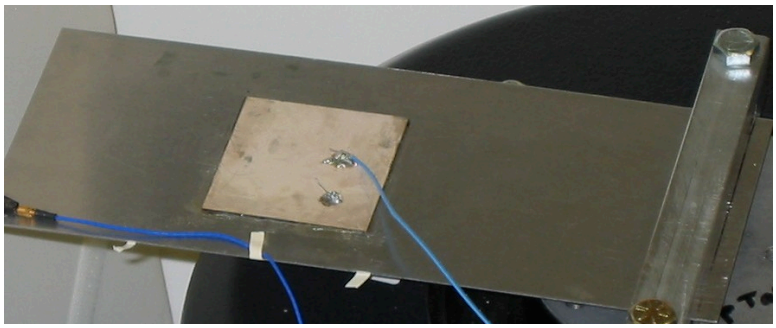

Figure 3.4: Piezoelectric patch glued to the plate to suppress first mode of vibration

There is a large difference observed between the frequencies obtained from ABAQUS and the experiment. This is believed to be because the boundary conditions in ABAQUS are considered to be a clamped edge at one end, which constrains all the translations (U_x,U_y and U_z) and rotations (ROT_x, ROT_y,ROT_z), while in the experiment it is not the case. The clamp is fixed on the shaker, which represents base excitation with the acceleration due to the mass of the shaker at the clamped end. This applies force in U_z direction during the experiment. Moreover, perfect bonding of the piezoelectric patch is assumed in the analytical model while it is not the case during the experiment. Perfect bonding of the piezoelectric patch to the controlled structure is an assumption ((16)). The density of the piezoelectric patch and the compliance of epoxy used to attach the patch also plays an important role in altering the natural frequencies of the plate. The clamp designed for the work is also not wide enough to give a perfect clamped boundary conditions on the clamped edge on the other degrees of freedom apart from the U_z DOF.

Various combinations of nodal loading are available for plate element and piezoelectric element is assumed to have four degrees of freedom, three translations in **x**, **y** and **z** directions, and VOLT in the direction perpendicular to the surface of the piezoelectric patch. The essential electromechanical equations for finite elements representing piezoelectric materials is summarized as:

$$(\mathbf{T}) = [\mathbf{c}](\mathbf{S}) - [\mathbf{e}](\mathbf{E}) \tag{3.21}$$

$$(\mathbf{D}) = [\mathbf{e}]^{\mathbf{T}}(\mathbf{S}) + [\epsilon](\mathbf{E}) \tag{3.22}$$

These equations are the usual structural and electrical constitutive equations as in Equations 3.1 and

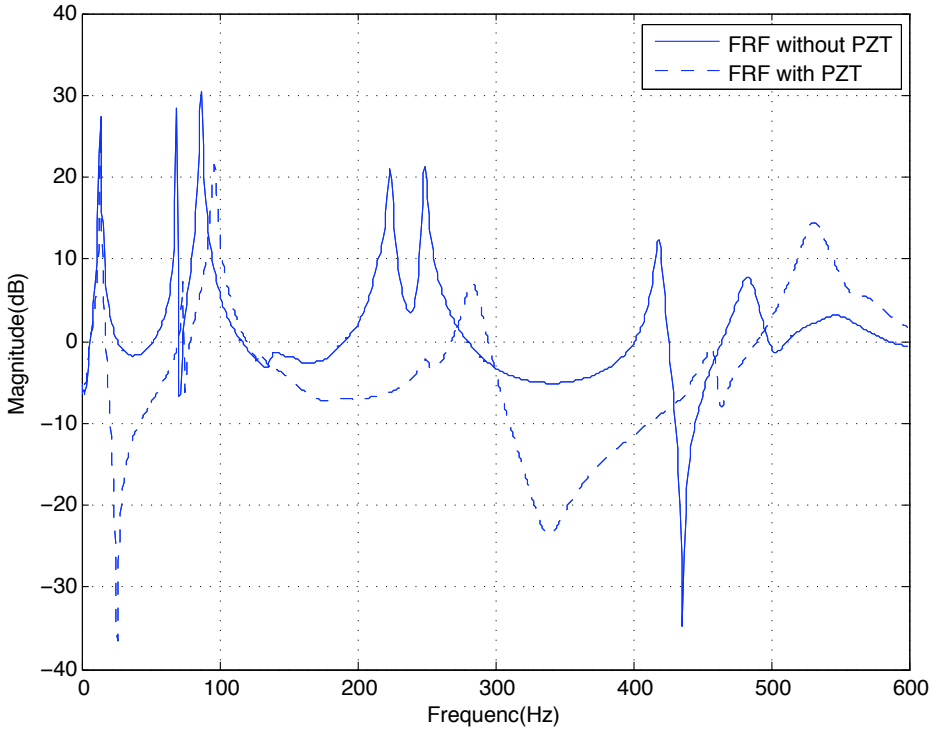

Figure 3.5: FRF with and without the piezoelectric patch on host structure

3.2, respectively. The element used in ABAQUS for piezoelectric patch has 8 nodes and the input data contains piezoelectric constant matrix, anisotropic compliance or elasticity matrix, orthotropic relative permittivity matrix and density of the patch. Density of Pz29 is 7640 $\frac{\text{kg}}{\text{m}^3}$. The other properties ((26)) for Pz29 are given below

$$\mathbf{s} = \begin{bmatrix} 17.0 & -5.78 & -5.78 & 0 & 0 & 0 \\ -5.78 & 17.0 & -5.78 & 0 & 0 & 0 \\ -5.78 & -5.78 & 22.9 & 0 & 0 & 0 \\ 0 & 0 & 0 & 54.1 & 0 & 0 \\ 0 & 0 & 0 & 0 & 54.1 & 0 \\ 0 & 0 & 0 & 0 & 0 & 45.6 \end{bmatrix} 10^{-12} \times \text{m}^2/\text{N} \tag{3.23}$$

$$\mathbf{d} = \begin{bmatrix} 0 & 0 & 0 & 0 & 640 & 0 \\ 0 & 0 & 0 & 640 & 0 & 0 \\ -240 & -240 & 575 & 0 & 0 & 0 \end{bmatrix} 10^{-12} \times \mathrm{m/N} \quad \frac{\epsilon}{\epsilon_o} = \begin{bmatrix} 1340 & 0 & 0 \\ 0 & 1340 & 0 \\ 0 & 0 & 1220 \end{bmatrix} \tag{3.24}$$

such that in general the material matrices and the required finite element matrices are interrelated as follows:

$$[\mathbf{c}] = [\mathbf{s}]^{-\mathbf{1}} \tag{3.25}$$

and

$$[\mathbf{e}] = [\mathbf{d}][\mathbf{c}] \tag{3.26}$$

The natural frequencies of the structure with the piezoelectric patch are greater than that of the actual structure. Attaching a piezoelectric patch adds stiffness to the host structures thus causing a shift in eigenvalues. Transfer functions generated with and without the piezoelectric patch attached to the host structure and are displayed in Figure 3.5

Table 3.3: Natural frequencies of the cantilever plate with piezoelectric patch

Set	Natural frequencies from ABAQUS	Natural frequencies from EXPERIMENT
1	16.08 Hz	14.0 Hz
2	100.04 Hz	73.5 Hz
3	129.17 Hz	96.0 Hz
4	384.25 Hz	250.0 Hz
5	392.05 Hz	284.0 Hz
6	672.65 Hz	531.0 Hz

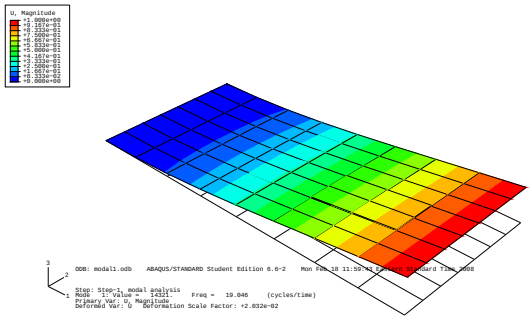

(a) First Mode

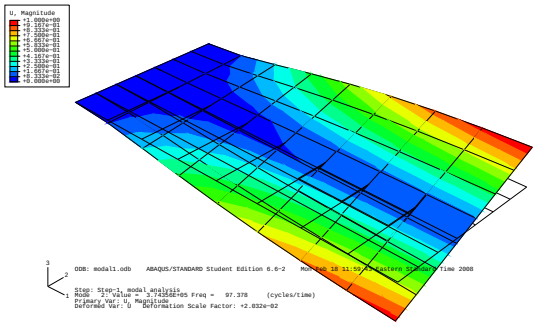

(b) Second Mode

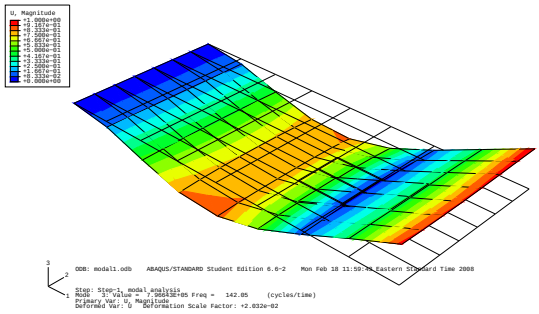

(c) Third Mode

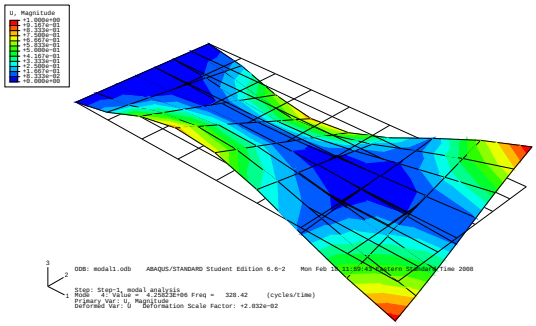

(d) Fourth Mode

Figure 3.6: Mode shapes of cantilever plate with piezoelectric patch from ABAQUS

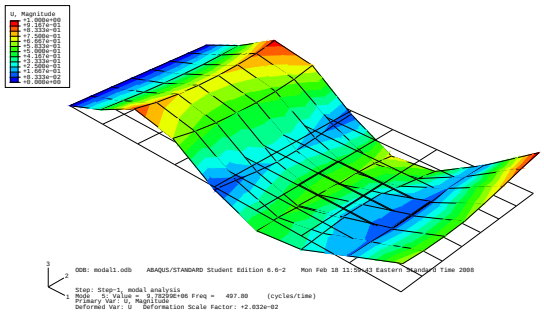

(e) Fifth Mode

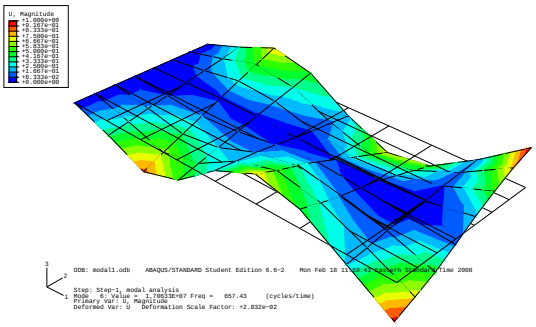

(f) Sixth Mode

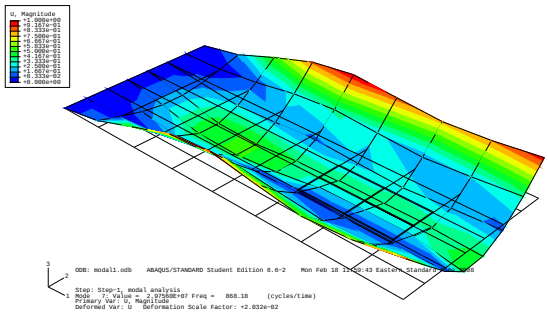

(g) Seventh Mode

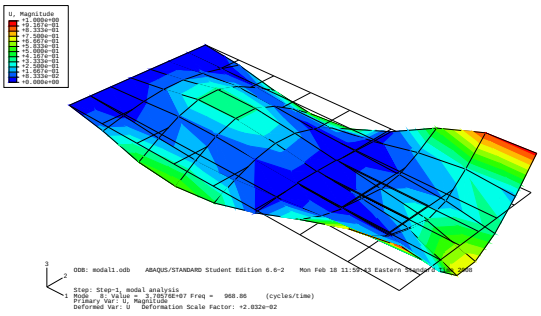

(h) Eighth Mode

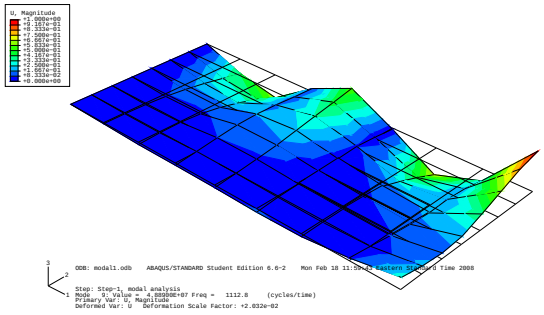

(i) Ninth Mode

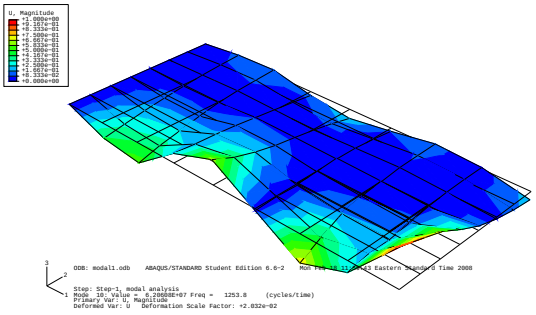

(j) Tenth Mode

Figure 3.6: Mode shapes of cantilever plate with piezoelectric patch from ABAQUS

Experiment Verification

4.1 Linearity Checks

A check for linearity on the shaker head is performed to make sure that that a linear model can be used. The shaker head or system could behave differently at different excitation levels and operating conditions. To test this effect of excitation amplitude, two sine sweeps of two different amplitudes, were performed from 0Hz to 1000Hz. The high amplitude of vibration was 10 times greater than the low amplitude of vibration. It was observed that the responses overlay each other, except small discrepancies at the peaks as shown in Figure 4.1. It was also observed that the excitation force is non-linear at very high amplitudes. Thus it was taken care that the amplitude of excitation does not go beyond the level of linear excitation amplitude.

4.2 Testing the Fixture

A test was devised to examine external influences on the test specimen like tightening effect of the bolts, joining the two pieces of the clamp, and whether the fixture was being excited at the natural frequencies of interest. Some had very serious impacts on the results and care was taken to avoid such effects and to run all the experiments under consistent conditions of torque on the bolts, amplitude of vibration, accelerometer placement etc.

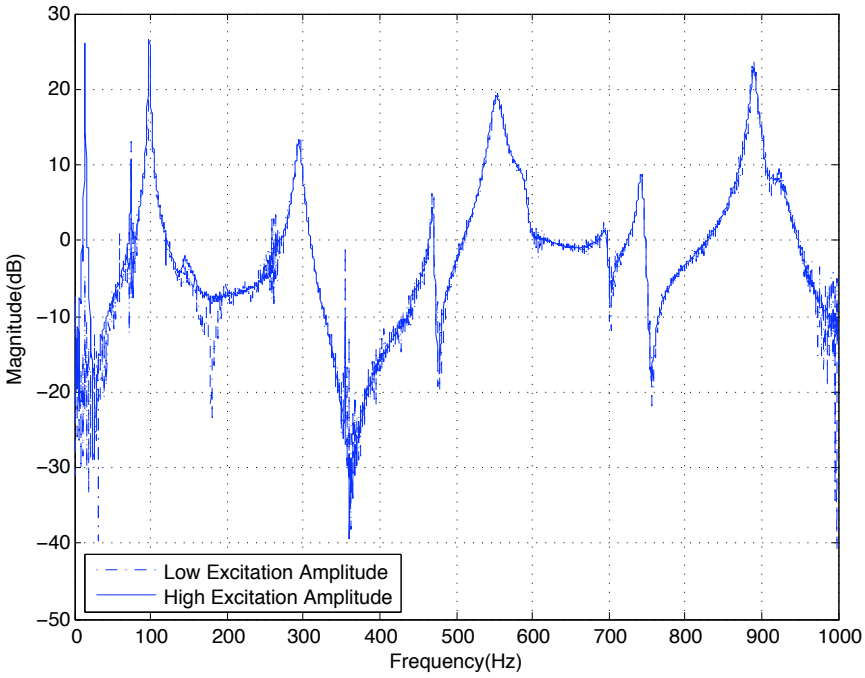

Figure 4.1: Linearity check of the shaker

4.2.1 Tightening Effect

The frequency response functions of the system when the bolts of the clamp are to hold the plate and over tightened are recorded. There is not much difference in the natural frequencies but the amplitude of the resonant peaks differ especially at higher frequencies as shown in Figure 4.2. This is likely due to an increase in dampening and slip for looser bolts.

Similar consequences are observed when one of the bolts of the holding device is loose. A loose bolt changes the boundary conditions of the system thus resulting in different natural frequencies and changed damping. Frequency response functions were attained for over tight and loose bolt cases and shown in Figure 4.3. The stiffness of the system is reduced thus resulting in frequency shift towards left.

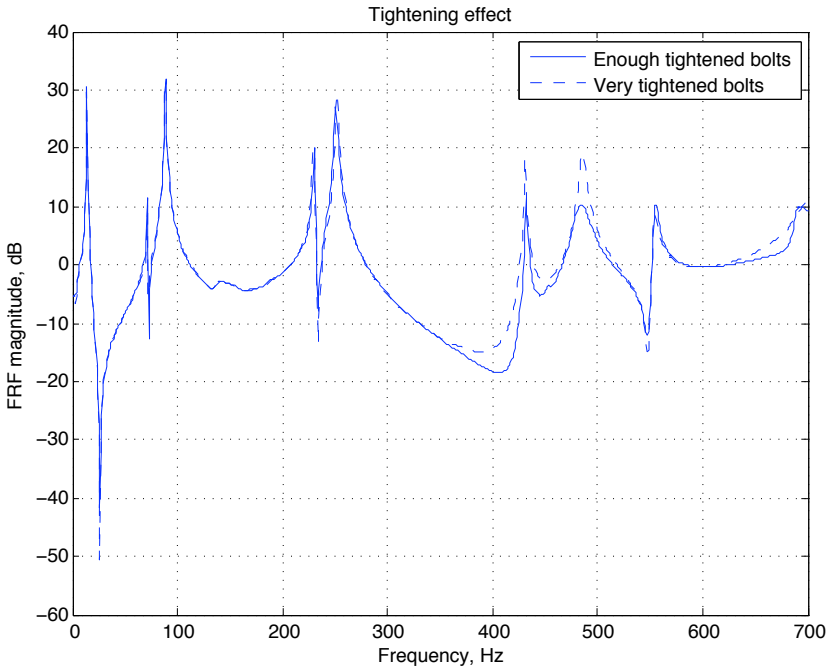

Figure 4.2: Tightening effects of bolts on FRFs

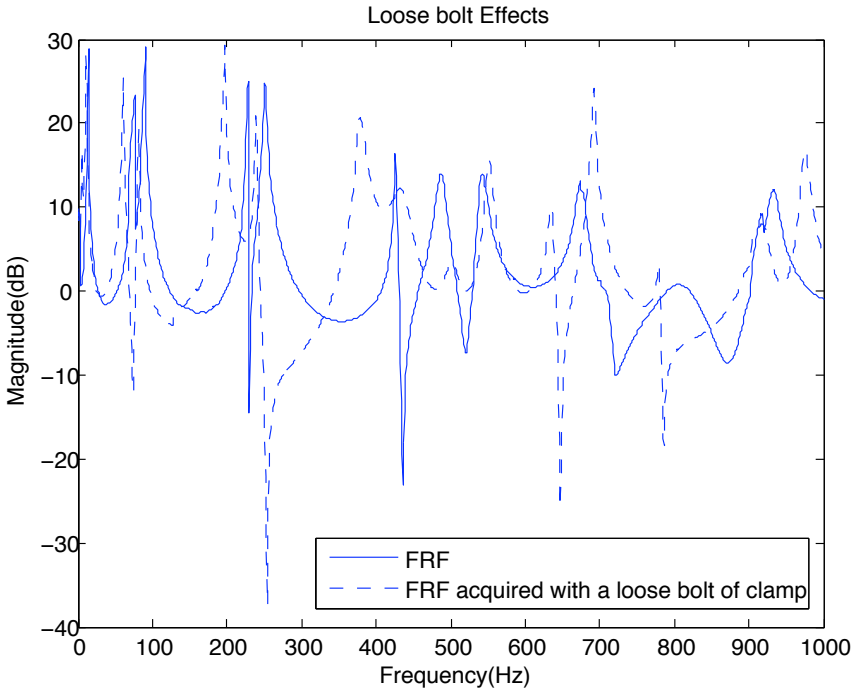

Figure 4.3: Effects on FRFs due to loosebolt

Passive Electrical Circuit

Piezoelectric transducers, in conjunction with appropriate circuitry, can be used as mechanical energy dissipation devices. Different linear components of circuit make the entire setup work differently. For example, if a resistor is placed in closed-loop to the PZT, the PZT will act as visco-elastic damper. If the circuit consists of a resistor and an inductor in series combined with inherent capacitance of the PZT, damped electrical resonance is created. Electrical resonance is then tuned to the structural resonance so that PZT acts as a tuned vibrational absorber device. This is especially used for single-mode shunt damping. To suppress multiple modes, this technique is challenged by the requirement that different piezoelectric patches be placed at different locations to curb the resonance amplitudes of multiple modes. To avoid these problems, multi-mode shunt damping technique is introduced ((27)) i.e., use of single piezoelectric patch to curb different modes. It includes one anti-resonant electrical circuits for each structural mode. In practical applications, a small variation in boundary conditions, structural load etc., would vary the resonant frequencies by significant value. Such variations would make it difficult to tune the electrical resonant frequency to the structural resonance thus detrimentally effecting the shunt damping performance.

Recently a new method of passive structural damping mechanism has been proposed, that depends upon the voltage produced from the piezoelectric patch. It is called “self-sensing vibration suppression.” This method depends only on the value of the piezoelectric voltage.

5.1 Self-Sensing Vibration Suppression

Self-sensing vibration suppression is a kind of switching control ((28)). Generally, a piezoelectric actuator is coupled to a circuit having a switch, and the switch is controlled to suppress vibration. But in self-sensing vibration suppression, instead of controlling a voltage supplier, a switch is closed/opened depending upon the voltage output from the piezoelectric patch while the host structure is vibrating.

When the switch is open, the electrical current does not flow and the charge density is constant. Thus Equation 3.22, indicates that the amplitude of vibration is proportional to the piezoelectric voltage.

$$(\mathbf{S}) = [\mathbf{e}]^{\mathbf{T}^{-1}}[\epsilon](\mathbf{E}) \tag{5.1}$$

At this state the piezoelectric element has high stiffness, and maximum potential energy. The state of vibration can thus be validated with the piezoelectric voltage, which is as easy as voltage-measurement approach. When the circuit is closed, the voltage decays and fluctuates and at this state it is switched to a low stiffness state, so that the potential energy is less than before. This difference in potential energy is released during the switching period from open to closed circuit. The component is kept short circuited until, the modal displacement reaches the equilibrium state. Now the piezoelectric element is switched back to the open circuit state and the entire cycle repeats. In short circuit case, the charge applied is equal to the negative of charge generated by the actuators deflection. In other words, there is no charge built up on the actuator. In our case, piezoelectric actuator is shunted across with diodes as shown in Figure 5.1.

5.1.1 Diodes

Diodes are very non-linear elements and thus the vibration amplitude is reduced due to introduction of non-linearity into the system. The advantage of this circuit has all the advantages of passive damping into account. Now, to drain the electrical energy produced from the piezoelectric patch, these diodes are connected to the wire soldered on the piezoelectric patch as shown in Figure 5.1.1

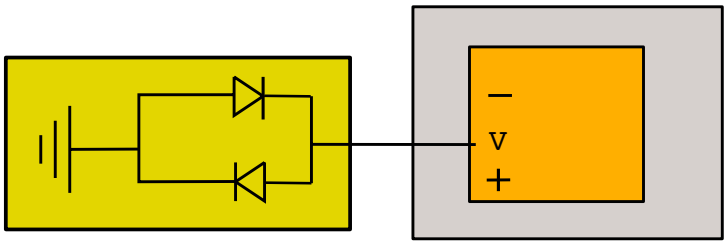

Figure 5.1: Disruptive diode circuit

In the electrical circuit, one diode is forward biased and the other is reverse biased, since the diode is a component that restricts directional flow of current. If an external voltage is placed across the diode with the same polarity as the built-in potential, the diode acts as an insulator. If the external voltage is applied across the diode with opposite polarity as the built-in potential, diodes do not conduct for a period of time and then starts conducting as the voltage potential applied is gradually increased. This voltage is approximately 0.33V-0.35V and is known as 'breakdown voltage' of the diode. When the voltage on the piezoelectric patch reaches the breakdown voltage, the diodes start conducting and he charge on it is drained. This affects the stress in the patch effectively reducing the stiffness of the system. Schottky diodes have very low breakdown voltage and are also fast switching. These diodes were used in our experiment. The forward current versus forward voltage characteristics of a diode are expressed with the diode Equation 5.2

$$I(t) = I_o(e^{\frac{\mathbf{V(t)}}{\mathbf{V_{th}}}} - 1) \tag{5.2}$$

where $I(t)$ and $V(t)$ are forward current and voltage across the diode, I_o is the leakage current, and V_{th} is the thermal voltage given by

$$V_{th} = \frac{kT}{q} = 25.85\text{mV} \tag{5.3}$$

where k is the Boltzmann constant (1.38×10^{-23}J/K), T is the temperature in ($^{\circ}$K) and q is the

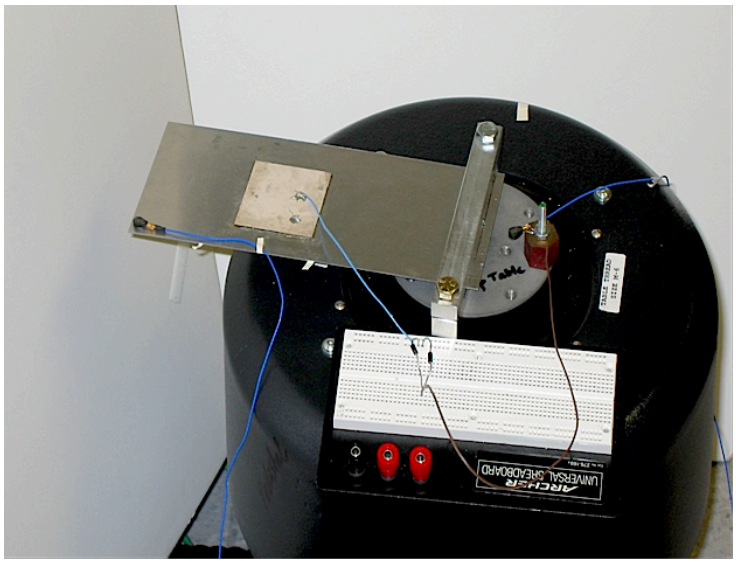

Figure 5.2: Experimental setup

elementary charge $(1.60217 \times 10^{-19}$coloumbs$)$. When a P-N junction diode is reverse biased it is generally approximated that there is no current flow through the diode until the breakdown voltage is reached. However, this is not true and there is still small leakage current I_0, which is usually a few μA. A diode's I-V characteristic can be approximated by two regions of operation. The diode will become conductive as soon as the breakdown voltage is reached as shown on Figure 5.1.1.

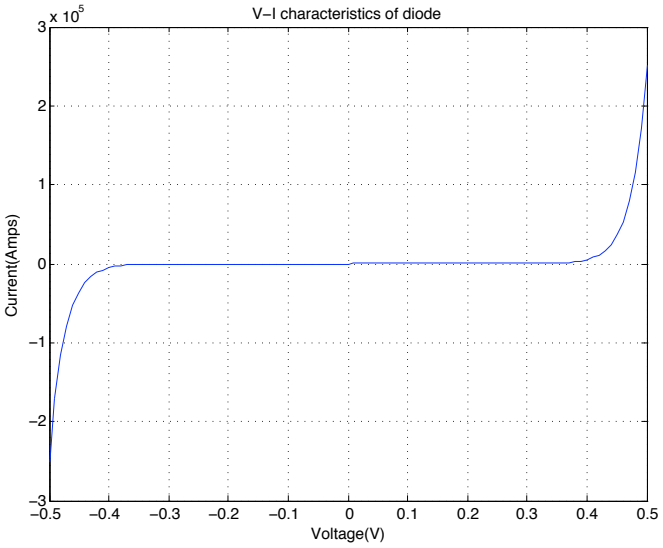

Figure 5.3: V-I characteristics of diode

5.2 Modal Testing

Modal testing has been performed to find the transfer function between each sensor and the input. Much of the early work in the control of smart structural systems was performed on single-input single-output (SISO) systems ((29)). These SISO systems are relatively simple. Even for a relatively small number of sensors, multivariable systems significantly increase the complexity of the system identification and control design. Using large number of closely spaced lightly damped modes is time consuming and difficult modeling process. Parameter variations, incorrect assumptions and inexact boundary conditions increase the difficulty of modeling.

A single-input and multi-output (SIMO) technique has been used for this case. The input to the smart structure is force from the electromagnetic shaker. The output, is either acceleration of the plate placed at the free end or the voltage from the piezoelectric patch. Digital signal processing unit, SIGLAB, was used to measure the acceleration using an accelerometer and voltage from the bridge circuit as shown in Figure 5.4, where C_p is the capacitance of the piezoelectric patch. C_1 is

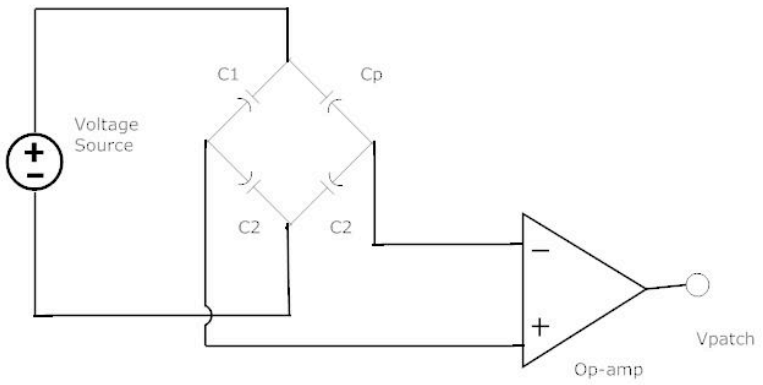

Figure 5.4: Bridge circuit to measure the voltage from the piezoelectric patch

a capacitor whose capacitance is equal to the capacitance of the piezoelectric patch, C_2 is another capacitor which is chosen to be approximately 10 times greater than C_p. Voltage source (V_s) in the circuit will be the voltage from the piezoelectric patch due to the disturbance caused. The operational amplifier used here has the capability to condition and amplify the voltage difference between points B and D. It also has a built in circuit that returns the difference in the voltage. The

voltage measured out of the op-amp is the voltage generated by the piezoelectric patch, V_p in terms of the voltage supplied given as

$$V_p = \frac{C_p + C_2}{C_p} V_s \tag{5.4}$$

Now, a virtual network analyzer is used to obtain the time history data of the acceleration and the voltage with a sampling frequency of 500 Hz. 35 time history records were taken. Frequency response functions between acceleration of the base excitation and acceleration of the plate and acceleration of the base excitation and voltage from the piezoelectric patch are then estimated as 5.5 and 5.6 respectively.

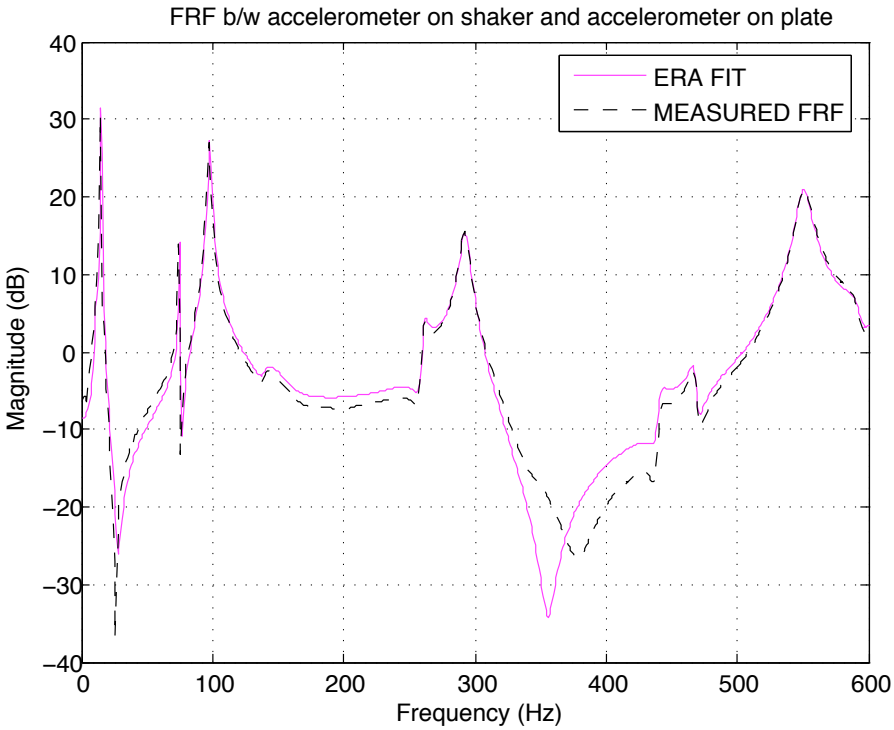

Figure 5.5: FRF between shaker input and the acceleration on plate

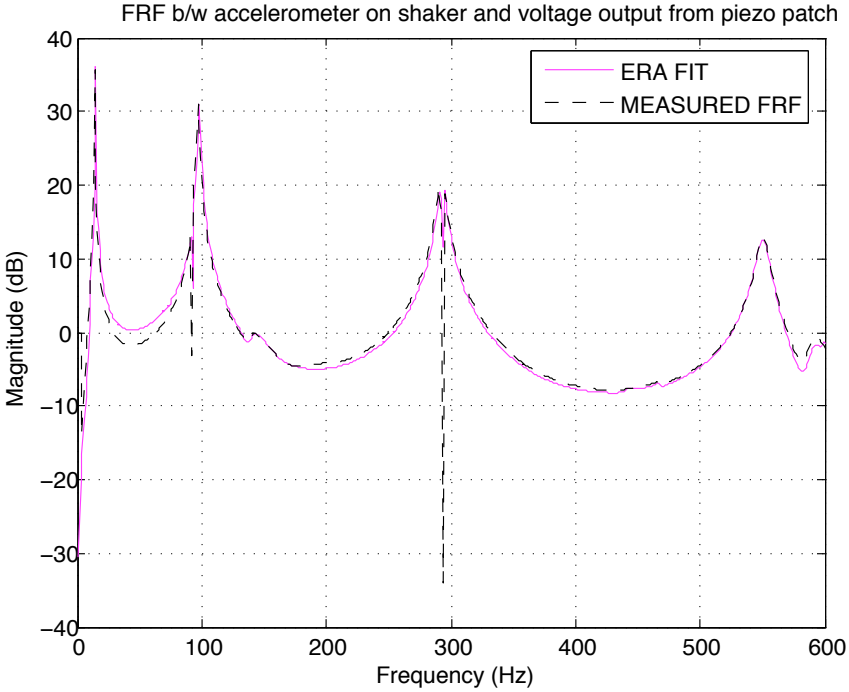

Figure 5.6: FRF between shaker input and the voltage from piezoelectric patch

The Eigenstructure Realization Algorithm (ERA) coded in EZERA was applied to the data to estimate the state space model of an LTI (Linear time invariant) system. A state space model is then built in MATLAB, using the matrices state matrix (A), output matrix (B), input matrix (C) and feed forward matrix (D) which represent the physical system. Because the frequency response functions are just the fast fourier transform (FFT) of the impulse response function, an impulse response function is determined from the state space model attained. The frequency response functions of the identified system were then compared to the response functions attained experimentally and are plotted in Figures 5.7 and 5.8.

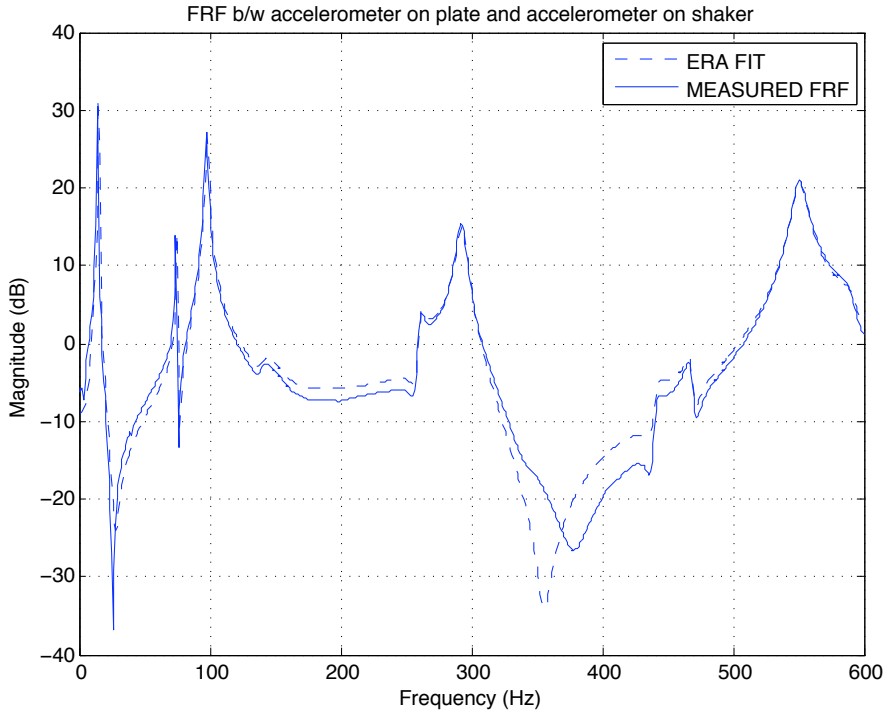

Figure 5.7: Measured vs Identified FRF b/w accelerometer on the shaker and accelerometer on the plate

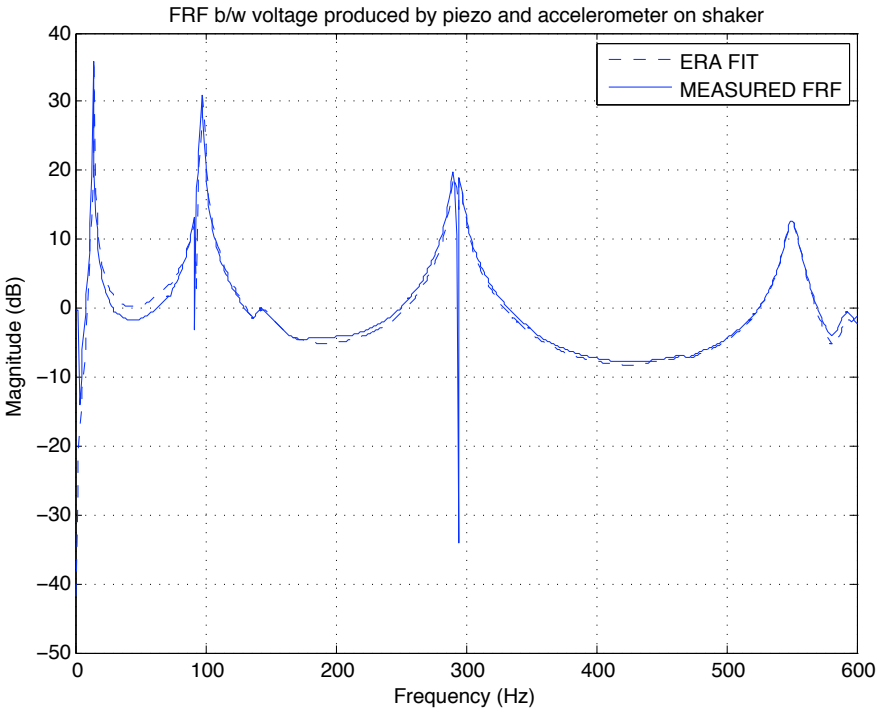

Figure 5.8: Measured FRF vs Identified FRF b/w accelerometer on the shaker and voltage from the piezoelectric patch

Simulink Block Diagram

In order to design and implement the control system, it is necessary to identify the system characteristics. This is obtained experimentally and analytically.

6.1 Numerical Modeling

Due to polarization and the anisotropic structure of the PZT material, piezoelectric properties depend on the relative direction to the poling axis. If the cantilevered plate is assumed to vibrate in pure bending, then the stress in the piezoelectric patch is confined to the stress in x-direction. Thus the electro-mechanical Equations 3.8 and 3.9 reduce to scalar equations as:

$$S_1 = s_{31}^E T_1 + \frac{d_{31} V_3}{t_p} \tag{6.1}$$

$$Q_3 = d_{31} A_p T_1 + C_p V_3 \tag{6.2}$$

where $C_p = \frac{\epsilon_{33} A_p}{t_p}$. Material properties of the piezoelectric patch that are used, are given in Equations 3.23 and 3.24. A physics-based electro-mechanical model of the system was then developed in Simulink is shown in Figure 6.1. Three major parts of the model are: model representation of the structure, representation of piezoelectric patch, and the electrical model of the diode shunt circuit.

Initially the circuit is assumed to be open and the displacement due to the external force applied is calculated. This calculated displacement is used to find the stress and then the voltage out of the piezoelectric patch. The voltage is passed through the diode equations which builds the charge over

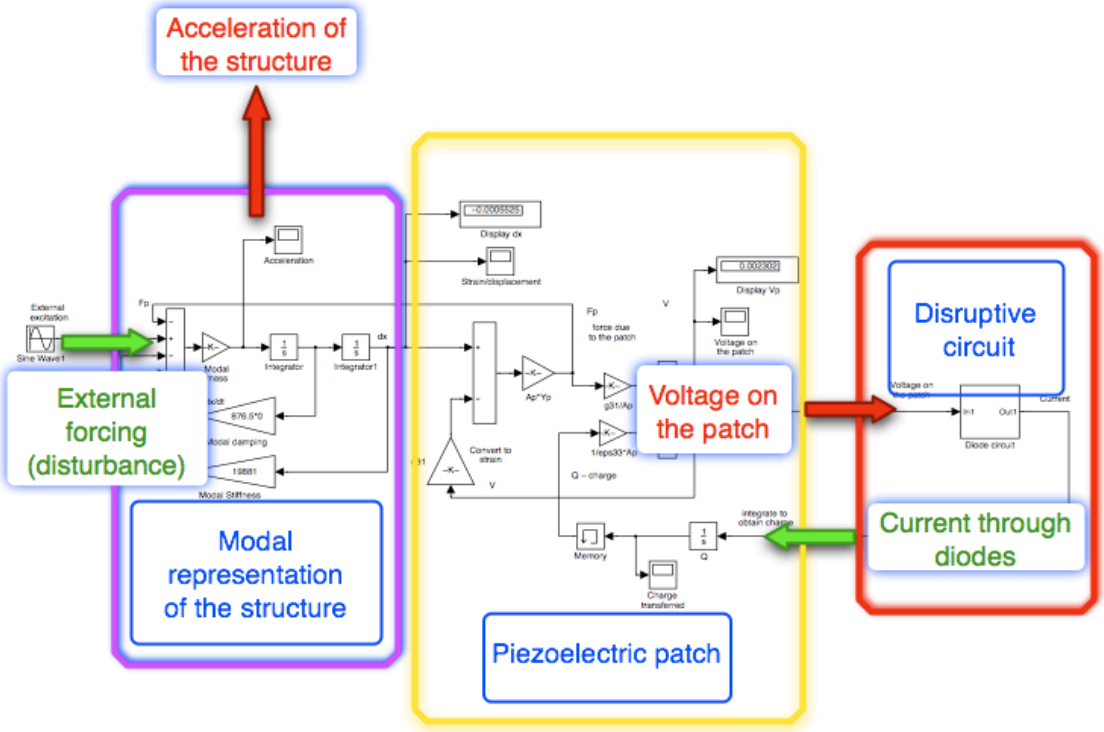

Figure 6.1: System model in Simulink.

the piezoelectric patch. All these terms are coupled together and the Simulink block diagram is developed in one-dimension.

6.2 System Modeling

An FE model of the plate with the piezoelectric patch was generated in ABAQUS. All electrical potential degrees of freedom that are placed on electrode surfaces of the patches are reduced such that only one potential master degree of freedom exists on each side of the piezoelectric patch. The discretized coupled structural and piezoelectric field equations are given in terms of nodal displacement **x** and nodal electric potential **v** by (30) as

$$\begin{bmatrix} M_{uu} & 0 \\ 0 & 0 \end{bmatrix} \begin{bmatrix} \ddot{\mathbf{x}} \\ \ddot{\mathbf{v}} \end{bmatrix} + \begin{bmatrix} K_{uu} & K_{uv} \\ K_{vu} & K_{vv} \end{bmatrix} \begin{bmatrix} \mathbf{x} \\ \mathbf{v} \end{bmatrix} = \begin{bmatrix} \mathbf{F}_1 \\ \mathbf{F}_2 \end{bmatrix} \tag{6.3}$$

The right hand side of the Equation 6.3 are the external forces ($\mathbf{F}_1$) and voltages or charges ($\mathbf{F}_2$) applied to the piezoelectric patch. The stiffness matrix contains coupled piezoelectric and structural stiffness while the mass matrix comprises only initial inertia of the structure. The nodes on the surface between the patch and plate, are coincident and were merged into one set of nodes containing all the degrees of freedom of the two sets. The plate element has translations and rotations while the patch has translations and electric potential as degrees of freedom. After the nodes are merged, the output node has all translations, rotations and also electric potential as degrees of freedom.

After the finite element modeling of the plate with the piezoelectric patch is formed with ABAQUS, the stiffness and mass matrices are obtained and exported into Matlab. Re-writing Equations 3.21 and 3.22 in a matrix form-

$$\begin{bmatrix} T \\ D \end{bmatrix} = \begin{bmatrix} \mathbf{c} & -\mathbf{e} \\ \mathbf{e^T} & \epsilon \end{bmatrix} \begin{bmatrix} S \\ E \end{bmatrix} \tag{6.4}$$

The significance of the above equation is that it generates the stiffness matrix of the piezoelectric patch. The vector on the left hand side of the equation resembles a force vector $[F_1, F_2]^T$. This

particular equation is a static deflection case and thus the stiffness matrix attained from ABAQUS, with the host structure and the piezoelectric patch is similar the coupled matrix as in equation 6.4.

Now from equations 6.3 and 6.4

$$\begin{bmatrix} M_{uu} & 0 \\ 0 & 0 \end{bmatrix} \begin{bmatrix} \ddot{\mathbf{x}} \\ \ddot{\mathbf{v}} \end{bmatrix} + \begin{bmatrix} C & 0 \\ 0 & C^{VH} \end{bmatrix} \begin{bmatrix} \dot{\mathbf{x}} \\ \dot{\mathbf{v}} \end{bmatrix} + \begin{bmatrix} \delta\mathbf{c} & -\delta\mathbf{e} \\ \delta\mathbf{e}^T & \delta\epsilon \end{bmatrix} \begin{bmatrix} \mathbf{x} \\ \mathbf{v} \end{bmatrix} = \begin{bmatrix} \mathbf{F} \\ \mathbf{L} \end{bmatrix} \tag{6.5}$$

where C is the structural damping matrix and C^{VH} is the dielectric damping matrix. δ here represents differential. Rotational degrees of freedom at the clamped end are constrained while force is applied in U_z direction. On the right hand side of the equation F is the external force vector and L is applied nodal charge vector.

Thus, the stiffness and mass matrices extracted from ABAQUS are utilized to identify the system in Simulink. The only force applied on the entire system is the acceleration due to the shaker at the clamped end. Thus the entire matrix is written in terms of the nodes at clamped end, nodes throughout the structure and the nodes at the piezoelectric patch using Equation 6.6

$$\begin{aligned} &\begin{bmatrix} M_{cc} & M_{cr} & 0 \\ M_{rc} & M_{rr} & 0 \\ 0 & 0 & 0 \end{bmatrix} \begin{bmatrix} \ddot{\mathbf{x}}_\mathbf{c} \\ \ddot{\mathbf{x}}_\mathbf{r} \\ \ddot{\mathbf{v}} \end{bmatrix} + \begin{bmatrix} C_{cc} & C_{cr} & 0 \\ C_{rc} & C_{rr} & 0 \\ 0 & 0 & C^{VH} \end{bmatrix} \begin{bmatrix} \dot{\mathbf{x}}_\mathbf{c} \\ \dot{\mathbf{x}}_\mathbf{r} \\ \dot{\mathbf{v}} \end{bmatrix} + ... \\ &+ \begin{bmatrix} K_{cc} & K_{cr} & K_{cv} \\ K_{rc} & K_{rr} & K_{rv} \\ K_{vc} & Kvr & K_{vv} \end{bmatrix} \begin{bmatrix} \mathbf{x}_\mathbf{c} \\ \mathbf{x}_\mathbf{r} \\ \mathbf{v} \end{bmatrix} = \begin{bmatrix} \mathbf{F}_c \\ \mathbf{F}_r \\ \mathbf{L} \end{bmatrix} \end{aligned} \tag{6.6}$$

where subscripts c and r represent the degrees of freedom at the clamped end and the degrees of freedom at the other nodes. These matrices are solved for x_r and v degrees of freedom in Simulink.

The second and the third set of equations from the matrix Equation 6.6 are used in the block diagram. Equations are written in the following form to solve for x_r and v degrees of freedom.

$$\ddot{x_r} = M_{\text{rr}}^{-1}(-M_{\text{rc}}\ddot{x}_c - C_{\text{rc}}\dot{x}_c - K_{\text{rc}}x_c - C_{\text{rr}}\dot{x}_r - K_{\text{rr}}x_r - K_{\text{rv}}v) \tag{6.7}$$

and

$$V = K_{\text{vv}}^{-1}(-K_{\text{vr}}x_r - K_{\text{vc}}x_c) \tag{6.8}$$

The matrices attained from ABAQUS are very large and are difficult to use in Simulink because it increases the simulation time. Therefore these matrices are initially reduced using the Guyan Reduction Process ((31)). Subsequently the System Equivalent Reduction-Expansion process (SEREP) is used to reduce the model to 12 modes of vibration. A MATLAB code is written to reduce the matrices M_{uu} and K_{uu}, matrices corresponding to translational and rotational degrees of freedom only, using a transformation matrix, T_1. The transformation matrix is given as in Equation 6.9

$$T_1 = \begin{bmatrix} \phi_{\mathbf{r}} & \phi_{\mathbf{o}} \end{bmatrix} \tag{6.9}$$

where subscripts r and o stand for the retained and omitted degrees of freedom respectively and ϕ are mass normalized eigenvectors. Another transformation is generated during the process of SEREP and is called T_2. It is given as in Equation 6.10

$$T_2 = \begin{bmatrix} I & -{K_{ss}}^{-1}{K_{ms}}^{T} \end{bmatrix}^{T} \tag{6.10}$$

where s and m stand for slave and master degrees of freedom respectively. The degrees of freedom that are removed are slave degrees of freedom. The stiffness values associated with both translations, rotations and electric degrees of freedom are reduced using the transformation matrices obtained from the previous processes as shown below

$$K_{vc} = T_2 K_{vc} T_1 \qquad\qquad K_{cv} = T_1 K_{cv} T_2 \tag{6.11}$$

Lagrange Multipliers are applied on the clamped end. It is assumed that the forces or acceleration applied at the end of the clamp has same magnitude and phase at all the nodes. This assumption made the force application much simpler. After all other matrices are reduced, a multipoint constraint is set on the voltage degrees of freedom. The voltages are constrained to be the same at all the nodes using Lagrange Multipliers. This further reduces the matrices so that there is only one voltage degree of freedom representing the entire piezoelectric patch. This was required to connect

the diode Equation 5.2 to the voltage output from the piezoelectric patch.

Block diagram with all the equations mentioned above is as shown in the Figure 6.2.

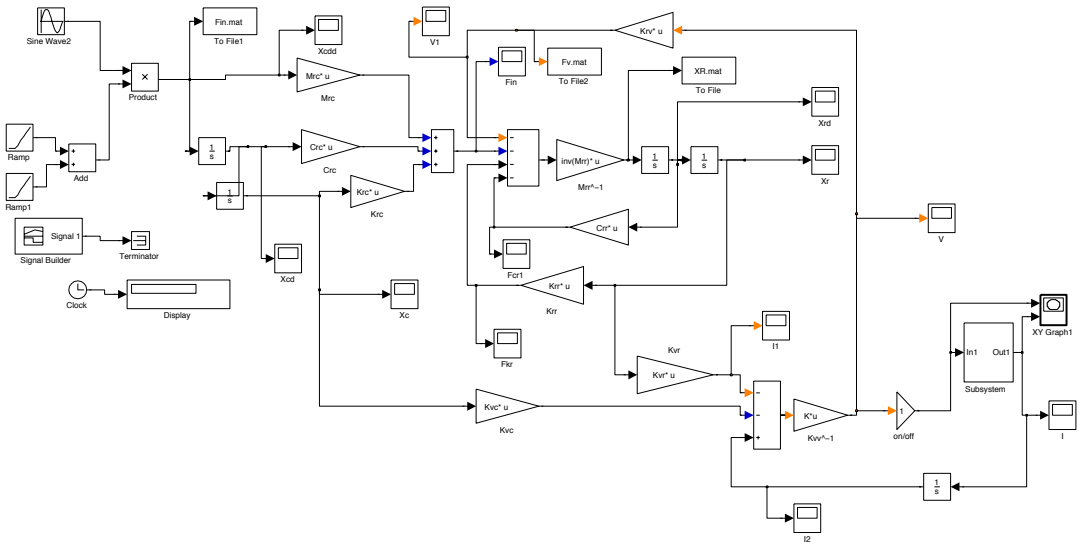

Figure 6.2: Block diagram from simulink

6.3 Model Correction

It is observed from the previous sections that the natural frequencies of the experimental and analytical model do not match. This is probably because of the difference in the boundary conditions. The analytical model assumes that the degrees of freedom at the fixture are perfectly clamped while that is not the case in the real experiment. The clamp used in the experiment is fixed so tightly at the bolts that it has bent at the center. Model correction can help match the analytical model with that of the experiment. Although this is not an ideal solution, it is necessary for evaluation of the controller.

In order to achieve this analytical correction using the model test data without destroying the FE modeled coupling of the plate with the piezoelectric patch, the stiffness matrix is assumed to be correct. Model correction is performed on the mass matrix while the damping matrix is generated

from identified mass matrix. Care is taken that model reduction methods, Guyan and Serep, have no impact on the model correction and vice versa.

The spectral matrix of the analytical model $\tilde{\mathrm{K}}$ is given in Equation 6.12

$$\tilde{\mathrm{K}} = (M_{\mathrm{uu}}^{-1})K_{\mathrm{uu}}(M_{\mathrm{uu}}^{-1}) \tag{6.12}$$

Matlab is used to determine the eigenvalues and eigenvectors of the spectral matrix. The eigenvalue matrix is given as follows

$$\Lambda = \phi^T \tilde{\mathrm{K}} \phi \tag{6.13}$$

The eigenvectors are corrected such that the eigenvalues of the analytical model match with those of the experimental model by dividing the vectors by a factor of a which is the ratio between the natural frequencies from the experiment and the finite element model. The modified mass matrix is obtained from the modified eigenvectors.

$$M = \frac{1}{a}\phi^{T^{-1}}\phi^T\frac{1}{a} \tag{6.14}$$

The damping matrix is obtained from the damping ratios determined from the experimental FRF and the eigenvalues and eigenvectors acquired from the stiffness matrix and model corrected mass matrix.

$$C_{\mathrm{rr}} = \begin{bmatrix} 2\zeta_1\omega_1 & 0 & 0 & ..... \\ 0 & 2\zeta_2\omega_2 & 0 & ..... \\ .... & ..... & ..... & ..... \\ 0 & 0 & 0 & 2\zeta_n\omega_n \end{bmatrix} \tag{6.15}$$

where n is the number of modes retained after model reduction. The final damping matrix is thus given in Equation 6.3.

$$C = \frac{1}{a}\phi^{T^{-1}}C_{\mathrm{rr}}\phi^T\frac{1}{a}$$

(6.16)

Natural frequencies of the model before and after model correction are given in Table 6.1

Table 6.1: Natural frequencies of the plate with piezoelectric patch before and after model correction

Set	NFs from ABAQUS (Hz)	NFs after Model-correction (Hz)
1	19.046 Hz	13.998
2	97.378 Hz	68.977
3	142.05 Hz	86.999
4	328.42 Hz	224.000
5	497.80 Hz	249.999
6	657.43 Hz	418.002
7	868.17 Hz	483..999
8	968.85 Hz	702.002
9	1112.83 Hz	794.001
10	1253.8 Hz	902.000

Results

7.1 Results from Experiment

In order to demonstrate the concept of diode shunt, an experimental test was performed on the clamped-free aluminum plate with and without the shunt. The goal of the experiment was to control the first and two-stripe mode of the plate using a disruptive diode circuit (Figure 5.1). Only one piezoelectric patch is used as a sensor and actuator. For resonant shunt vibration, FRFs were conducted performing Sinusoidal frequency sweeps and investigated the effectiveness of the proposed approach. Input of the FRF is the signal from the accelerometer placed on the shaker head and the output is the signal obtained from the accelerometer placed on the free end of the specimen (rectangular plate). Frequency response functions at the first mode frequency is obtained by running a sine sweep between 13 Hz to 14.8 Hz with a frequency step of 0.2 Hz. Similarly for the two-stripe mode frequency, sine wave between 495 Hz to 505 Hz is swept with a frequency step of 0.1 Hz. The control level voltage is set so that the voltage generated from the piezoelectric patch is greater than 0.33 V, which is the breakdown voltage of the diodes.

The experiment was performed in three different configurations: (i) open circuit, (ii) short circuit and (iii) shunted using the diode circuit. Amplitude reduction of 3.1 dB was achieved in configuration with the diode circuit versus open circuit for the first mode as shown in Figure 7.1. For the two-stripe mode, amplitude reduction of 2.6 dB was achieved as shown in Figure 7.2. Also, a small shift in the frequency is observed because of the non-linear effects of the diode circuit. Baseline tests were performed to ensure that plate without the shunt operates in the linear regime

across the range of excitation levels.

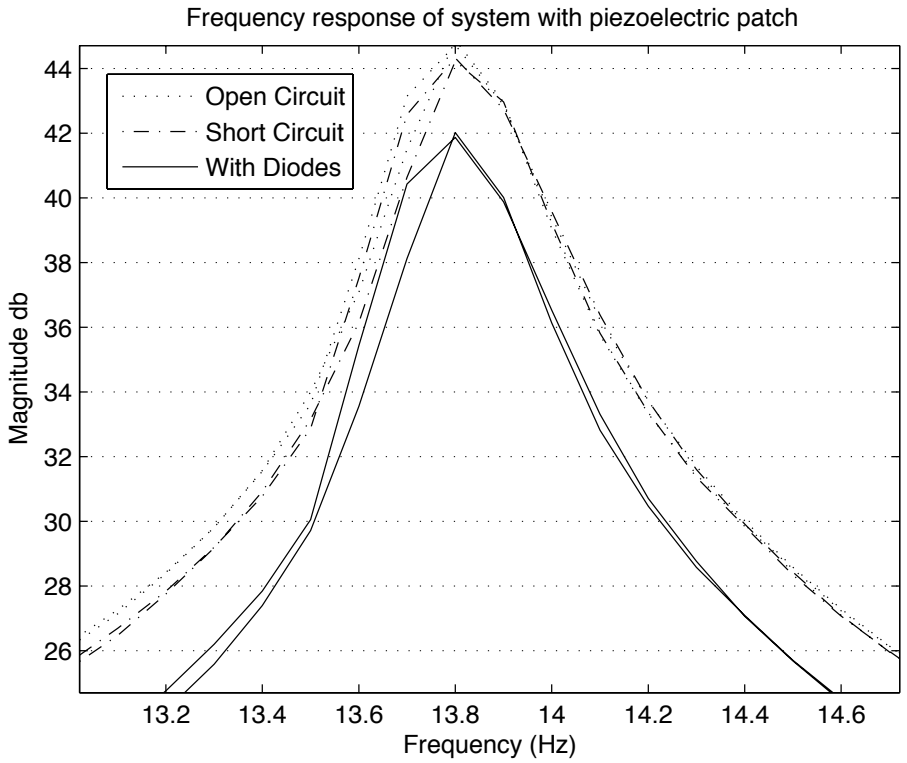

Figure 7.1: FRF at the first mode, with piezoelectric patch shunted across the diodes compared to open circuit

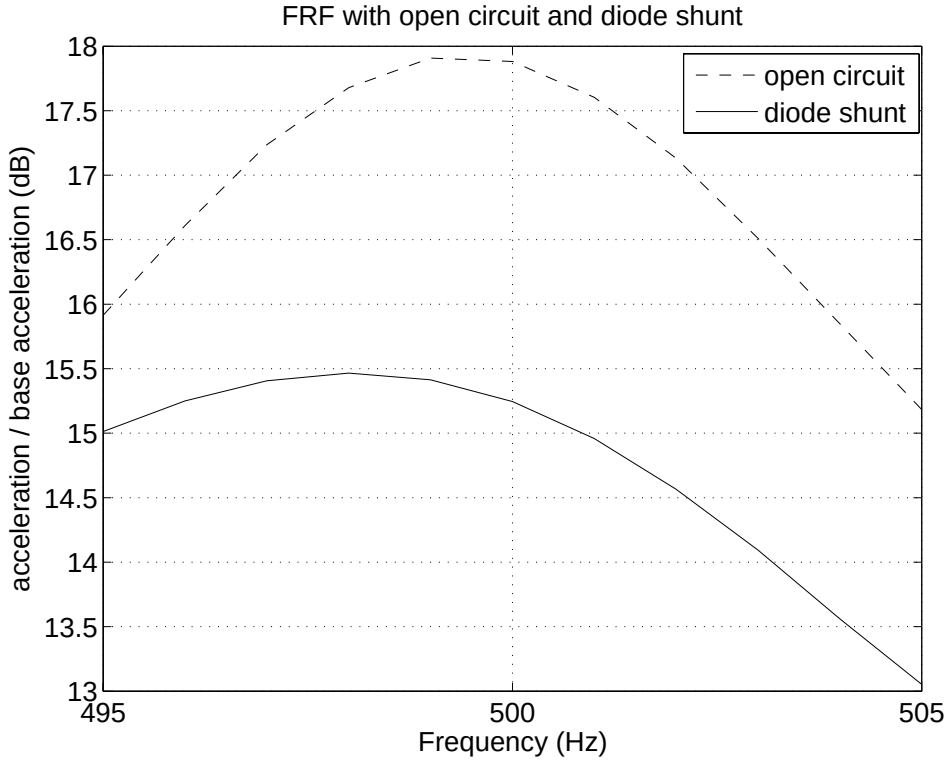

Figure 7.2: FRF at two-stripe mode, with piezoelectric patch shunted across the diodes compared to open circuit.

The open circuit and diode shunt circuit frequencies and magnitudes are given in Table 7.1. Because of the structural stiffness in parallel with the piezoelectric element, the total change in the

Table 7.1: Open and Diode shunt characteristics

Description	Freq(Hz)	Mag(dB)
Open Circuit	13.8	44.8
Short Circuit	13.8	41.9

Description	Freq(Hz)	Mag(dB)
Open Circuit	499.0	17.9
Short Circuit	497.5	15.3

system's stiffness is small; therefore, only small amounts of energy dissipation occurred. To better illustrate the nonlinear effects of the diodes, the voltage across the patch was recorded as a function of time for various excitation levels (see Figure 7.3). At lower amplitudes, voltage produced in the piezoelectric patch due to the mechanical disturbance is not enough to drive the diodes. At higher excitation amplitudes voltage in the patch exceeds forward bias voltage of the diodes, which causes one diode to conduct. This is because one diode is forwardly biased while the other is reversely biased. There will still be a small leakage current of a few μA current flowing through the reversely biased diode. The effects can be observed in Figure 7.3 as the voltage waveform changes its shape from a regular sinusoid to a clipped sinusoid with some additional harmonics.

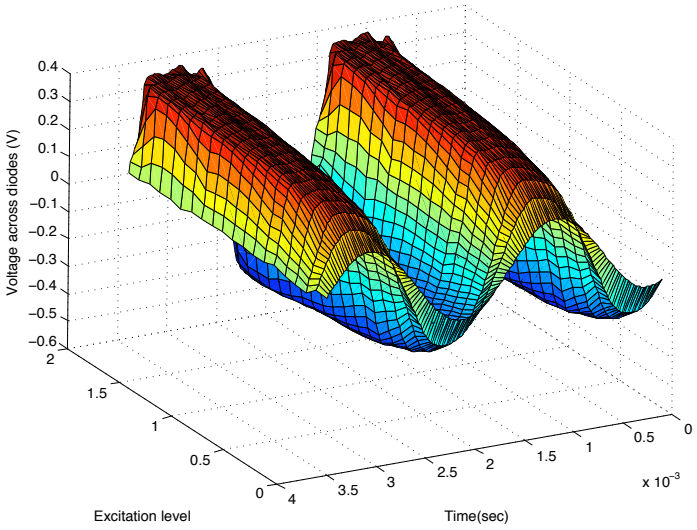

Figure 7.3: Diode voltage as a function of time at varying excitation levels.

7.2 Analytical Results

Analytical results are obtained from the Simulink model as shown in Figure 7.4. The force input to the system is the acceleration data obtained from the experiment at the clamped end. While performing the experiment an accelerometer was placed on the shaker head to measure the force input. Acceleration at different amplitudes was applied so that the voltage output from the piezoelectric patch slowly increases. A clipped sinusoid is obtained which is similar to the one obtained performing the experiment. There is no effect on the voltage produced until it reaches the forward voltage of the diode as shown in Figure 7.4.

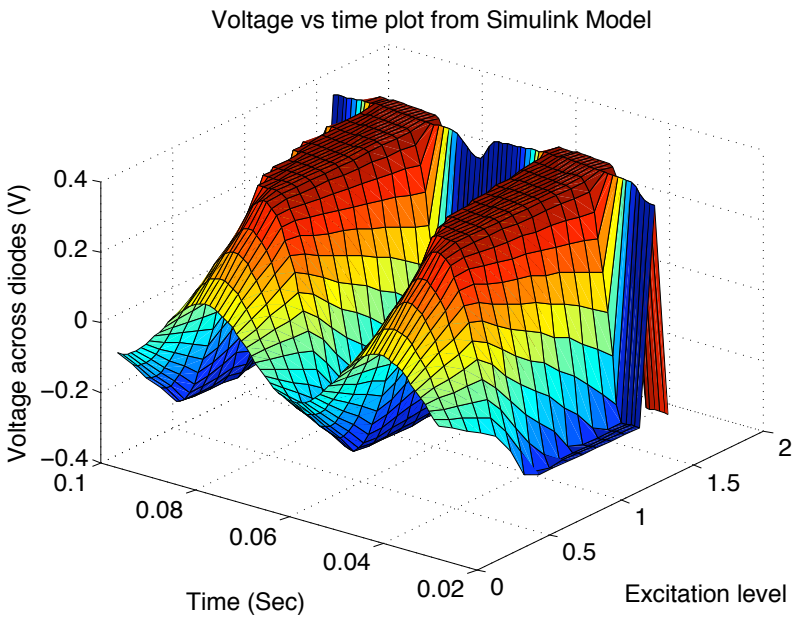

Figure 7.4: Voltage vs time plot from simulink block diagram

A MATLAB code was written to generate a sine sweep over required frequency range i.e. 0 Hz to 1000 Hz. This was imported into the Simulink block diagram using the Signal builder block. This simulation was run for 3 seconds and the acceleration input and the acceleration at the free end of the plate, $\ddot{x_r}$ from the Signal builder block are recorded. Then a Frequency Response Function is generated between acceleration input versus acceleration output by finding the auto-

spectrum density of the input and cross-spectrum density of the input and output in MATLAB. The H_1 transfer function generated from the analytical model is as shown in Figure 7.5.

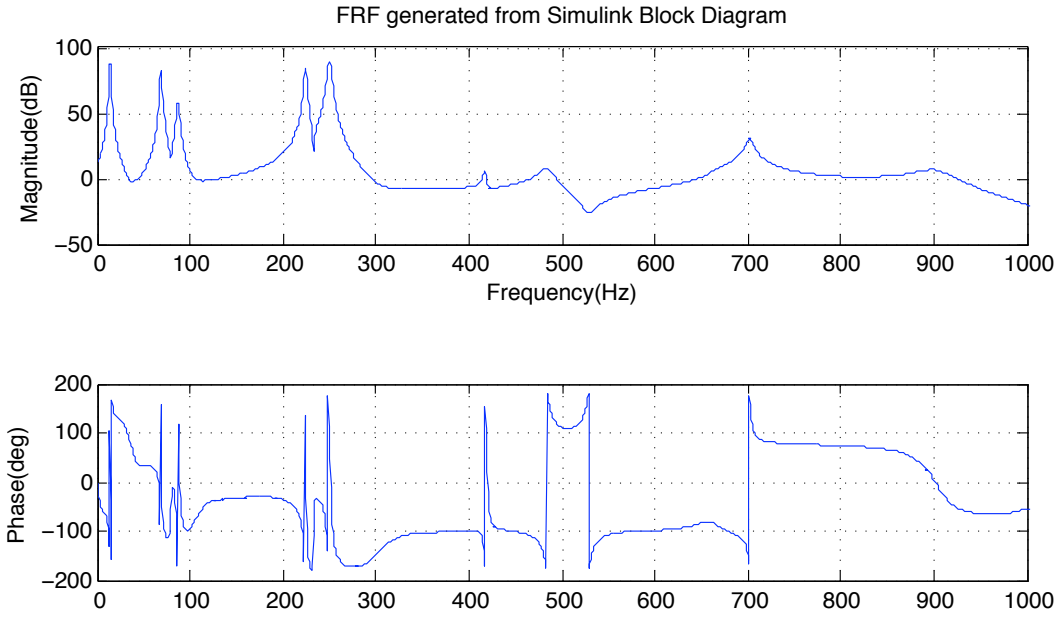

Figure 7.5: FRF obtained from simulink model

The simulation here were run in two different configurations, (i) Open Circuit and (ii) Closed Circuit. A sine wave with sufficient amount of amplitude to generate enough amount of voltage is the acceleration input to the model. Simulations are run at two different frequency ranges, 13 Hz to 15 Hz and 498 Hz to 500 Hz, with specific frequency interval of 0.1 Hz, and the magnitude of transfer function is recorded at each frequency. This test was run with and without the diodes and the results are obtained at the first mode and the two-stripe mode as shown in Figures 7.6 and 7.7 respectively.

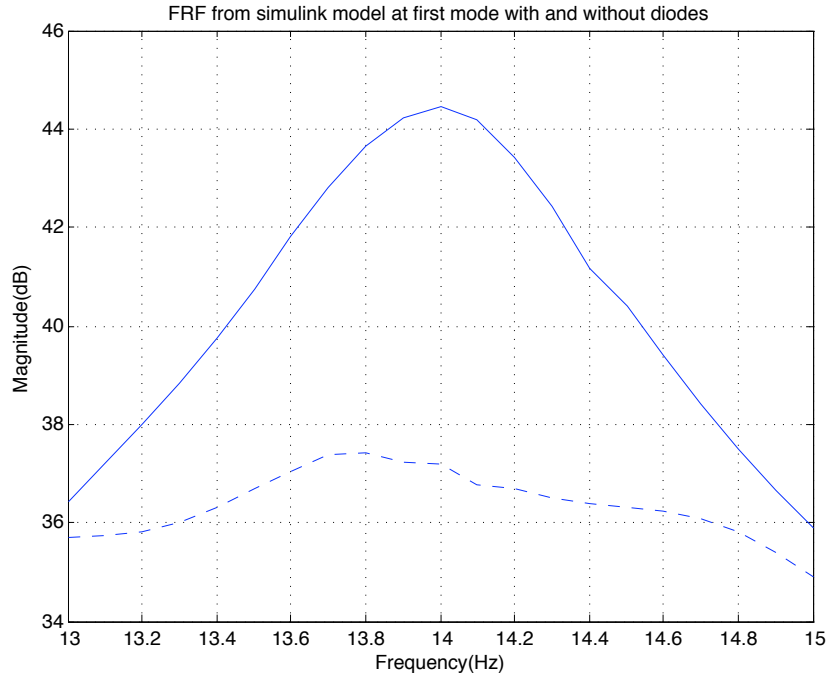

Figure 7.6: FRF at the first mode, with piezoelectric patch shunted across the diodes compared to open circuit from simulink model.

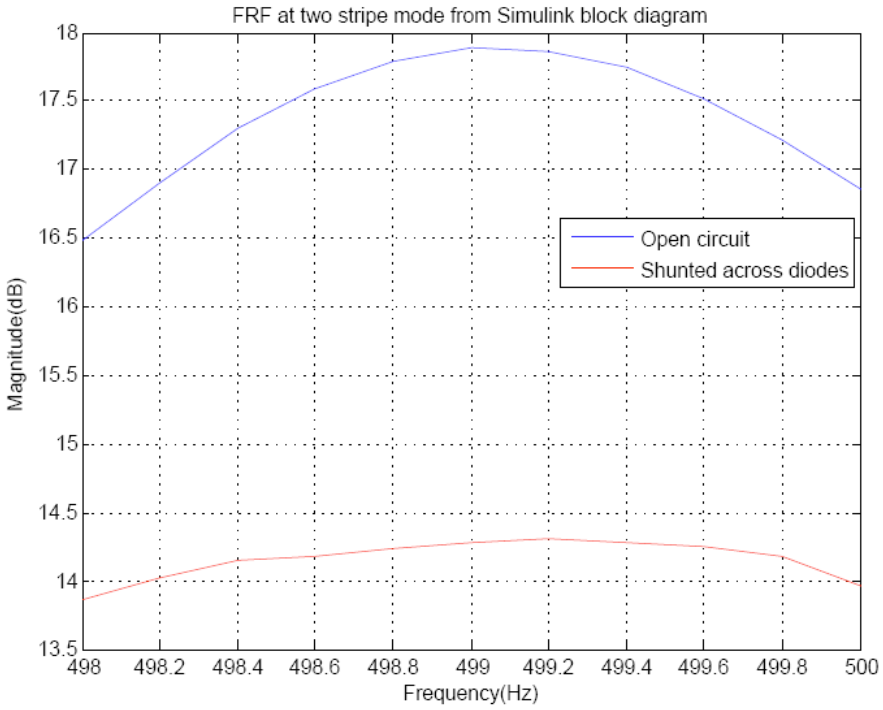

Figure 7.7: FRF at two-stripe mode, with piezoelectric patch shunted across the diodes compared to open circuit from simulink model.

7.3 Summary of Results

The experimental results for each mode of the plate are shown in Figures 7.2 and 7.1. The peak amplitude reductions are 3.1 dB and 2.6 dB at the first mode and two-stripe mode frequencies respectively. This technique is much easier than using linear circuit elements and avoids the problems of tuning the resistor and inductor circuits to the controlled structure's natural frequency.

Analytical results for each mode of the plate are shown in Figures 7.6. From the figure it is observed that there is a drop of 7.25 dB in magnitude at the first mode and 3.6 dB in magnitude at the two-stripe mode. The drop in amplitude of the peak from the analytical model are higher than that of the experimental. This probably could be because of the assumptions made in analytical model that the bonding between the piezoelectric patch and the plate is perfect. The stiffness and mass matrices obtained from ABAQUS are of a coarse mesh. Coarse mesh is used to keep the size of the matrices as low as possible. Clamp used in the experiment doesn't provide perfect clamping conditions. May be due to the above mentioned reasons the experimental results and analytical results doesn't match exactly. The percentage magnitude reductions are given in the Table 7.2.

Table 7.2: Percentage peak amplitude reductions from experiments and analytical model

Model	First Mode	Two-stripe Mode(Hz)
Experimental	30.00%	27.56%
Analytical	55.33%	34.00%

The response plot of the plate from simulink is obtained after transforming the output acceleration vector using the transpose matrices of the reduction processes used and is shown in Figure 7.8

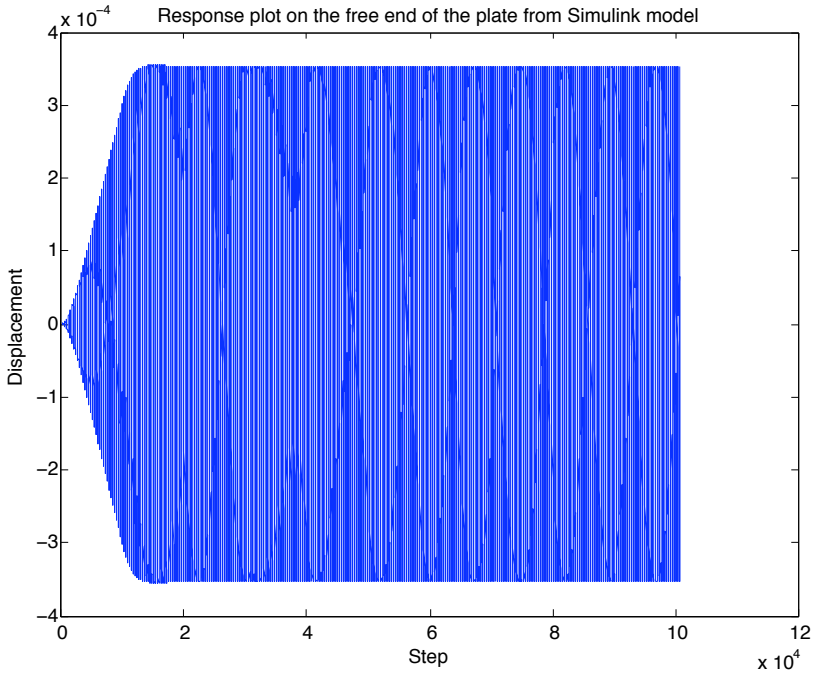

Figure 7.8: Response plot from Simulink Model

Conclusions

The design of an innovative electrical circuit to dampen the first and two-stripe modes of oscillation has been presented. For this intention, first a model of cantilever plate was designed. The analytical model identification techniques were implemented to determine the desired modes of vibration of the cantilever plate. The experimental frequency response function was then obtained by sweeping a sine wave for the required frequency range.

Modal analysis and a Sand Test were used to find a good location to bond the piezoelectric patch for receptive sensing and actuating. An electrical lead is soldered on to the piezoelectric patch to electrically connect the diode circuit. Frequency Response Functions are read using a SIGLAB. The FRFs are generated with and without the diode circuit. Sufficient peak drop is thus observed.

Then a finite element model of the plate with the piezoelectric patch is generated to attain the mass and stiffness matrices. SEREP and Static Condensation have been implemented to reduce the size of the plate model. These matrices are further used to identify the system in SIMULINK.

A combined electro-mechanical system model is developed using Simulink. An experiment is performed on a cantilevered plate with the piezoelectric patch. Preliminary results illustrating feasibility of the technique are presented.

8.1 Future Work

The research conducted for this thesis has shown the potential for future work in the area of smart material techniques and passive shunting with non-linear circuit elements. A further investigation

is required to accurately determine suitable diode to damp particular vibration mode. It has paved a way to evaluate other non-linear electrical elements available such as bipolar transistors etc., for potential designs.

The physics-based numerical model of the structure including the patch developed can be useful for the optimization of the circuit components to achieve better vibration suppression. The analysis can be further extended to more complex structures, like turbine blades etc. It can further be expanded in suppressing multiple modes.

Bibliography

[1] Crawley, E. F. and de Luis, J., "Use of Piezoelectric Actuators as Elements of Intelligent Structures," *AIAA*, Vol. 25, No. 10, 1987, pp. 1373–1385.

[2] H.S., T. and C.I., T., "Distributed piezoelectric sensor/actuator design for dynamic measurement/control of distributed parameter systems: a piezoelectric finite element approach," *Journal of Sound and Vibration*, 1990, pp. 17–34.

[3] G., G., J., B. M., and P., G., "Active Damping of a Beam Using Physically Collocated Accelerometer and Piezoelectric Patch Actuator," *Journal of Sound and Vibration*, Vol. 303, 2007, pp. 798–813.

[4] J.A., M. and E., G., "Design Impact of Piezoelectric Actuator Non-linearities," *Journal of Guidance Control and Dynamics*, Vol. 20, 1997, pp. 327–332.

[5] Edery-Azulay, L. and Abramovich, H., "Active Damping of Piezo-Composite Beams," *Composite Structures*, 2006, pp. 458–466.

[6] L., M., H., B., and H., O., "A Comparison Of Control Techniques For Large Flexible system," *Journal of Guidance, Control, and Dynamics*, Vol. 6, 1983, pp. 302–310.

[7] Seba, B., Ni, J., and Lohmann, B., "Vibration Attenuation using a Piezoelectric Shunt Circuit Based on Finite Element Method Analysis," *Smart Materials and Structures*, Vol. 15, June 2005, pp. 509–517.

[8] N.W., H., Chung, W. H., and Flotow, A. V., "Modelling of Piezoelectric Actuator Dynamics For Active Structural Control," *AIAA*, 1990, pp. 2242–2256.

[9] Hagood, N. W. and Flotow, V., "Damping of Structural Vibrations With Piezoelectric Materials and Passive Electrical Networks," *Journal of Sound and Vibration*, April 1991.

[10] Y., W. S., "Piezoelectric Shunts With a Parallel R-L Circuit For Structural Damping and Vibration Control," *Smart Materials and Structures*, Vol. 2720, 1996, pp. 259–269.

[11] J.J., H., "Multimodal Passive Vibration Suppression With Piezoelectric Materials and Resonant Shunts," *Journal of Intelligent Material Systems and Structures*, Vol. 5, 1994, pp. 49–57.

[12] Agnes, G. S. and Inman, D. J., "Nonlinear Piezoelectric Vibration Absorbers," *Smart Materials & Structures*, Vol. 5, 1996, pp. 704–714.

[13] J.J., H. and T.F., S., "A Self-Tuning Piezoelectric Vibration Absorber," *Journal of Intelligent Material Systems and Structures*, Vol. 5, 1994, pp. 559–566.

[14] G.S., A., "Development of a Modal Model For Simultaneous Active and Passive Piezoelectric Vibration Suppression," *Journal of Intelligent Material Systems and Structures*, Vol. 6, 1995, pp. 482–487.

[15] S., T. M. and W., W. K., "On the Structural Damping Characteristics of Active Piezoelectric Actuators With Passive Shunt," *Journal of Sound and Vibration*, Vol. 221, 1999, pp. 1–22.

[16] P., G. D. and L., A. G., "Structural Damping and Vibration Control via Smart Sensors and Actuators," *Vibration and Control*, Vol. 9, September 2003, pp. 1421–1452.

[17] Adachi, K., Awakura, Y., and Iwatsubo, T., "Active Control Effort of Hybrid Piezoelectric Absorber For Structural Control," *Applied Acoustics*, 2003, pp. 277–292.

[18] Tong, L., Sun, D., and Atluri, S. N., "Sensing and Actuating Behaviours of Piezoelectric Layers With Debonding in Smart Beams," *Smart Materials and Structures*, March 2001, pp. 713–723.

[19] S., T. H. and Q., F. H., "A Study of Segmentation of Distributed Piezoelectric Sensors and Actuators," *Journal of Sound and Vibration*, 1994, pp. 247–259.

[20] Halim, D. and S.O., R. M., "An Optimization Approach to Optimal Placement of Collocated Piezoelectric Actuators and Sensors on a Thin Plate," *Mechatronics*, Vol. 13, July 2001, pp. 27–47.

[21] Peng, F., G., A. N., and Hu, Y.-R., "Actuator Placement Optimization and Adaptive Control of Plate Smart Structures," *Journal of Intelligent Material Systems and Structures*, Vol. 16, March 2005, pp. 263–271.

[22] Dosch, J. J. and Inman, D. J., "A Self Sensing Piezoelectric Actuator For Collocated Control," *Intelligent Material Systems and Structures*, Jan 1992.

[23] Han, J.-H. and Lee, I., "Optimal Placement of Piezoelectric Sensors and Actuators For Vibration Control of a Composite Plate Using Genetic Algorithms," *Smart Materials and Structures*, Vol. 8, January 1999, pp. 257–267.

[24] Ayers, J. P., Greve, D. W., and Oppenheim, I. J., "Energy Scavenging for Sensor Applications using Structural Strains," *Smart Materials and Structures*, Vol. 5057, 2003, pp. 364–375.

[25] Main, J. A. and Garcia, E., "Piezoelectric Stack Actuators and Control System Design: Strategies and Pitfalls," *Journal of Guidance, Control, and Dynamics*, Vol. 20, No. 3, May-June 1997, pp. 479–485.

[26] Heinonen, E., Juuti, J., and Jantunen, H., "Characteristics of Piezoelectric Cantilevers Embedded in LTCC," *Journal of the European Ceramic Society*, April 2007, pp. 4135–4138.

[27] A.J., F. and S.O.R., M., "Adaptive Piezoelectric Shunt Damping," *Smart Materials and Structures*, Vol. 12, January 2002, pp. 36–48.

[28] Makihara, K., Onoda, J., and Minesugi, K., "A Self-Sensing Method for Switching Vibration Suppression with a Piezoelectric Actuator," *Smart Materials and Structures*, Vol. 16, February 2006, pp. 455–461.

[29] Butler, R. and Rao, V., "A State Space Modeling and Control Method For Multivariable Smart Structural Systems," *Smart Materials and Structures*, April 1996, pp. 386–399.

[30] Becker, J., Fein, O., Maess, M., and Gaul, L., "Finite Element-based Analysis of Shunted Piezoelectric Structures For Vibration Damping," *Computers and Structures*, Vol. 84, No. 31-32, December 2006, pp. 2340–2350.

[31] J., G. R., "Reduction of Stiffness and Mass Matrices," *AIAA*, Vol. 3, No. 280, 1965.